Online Appendix for "Timing Search"[1]

Contents

[1]Hanbaek Lee, University of Cambridge, Email: hl610@cam.ac.uk

A Theory and microfoundations

A.1 One-sided timing search

The one-sided timing search problem considers an agent who observes market conditions at Poisson rate λ and chooses when to act. With i.i.d. payoffs, the reservation value satisfies the standard McCall equation

$$rv^* = -c + \lambda \int_{v^*}^{\bar{v}} (v - v^*)\, dF(v),$$

and timing search is isomorphic to cross-sectional search.

Under Ornstein–Uhlenbeck payoffs ($dv = \theta(\bar{v} - v)dt + \sigma\, dW$), two results emerge with no cross-sectional analog. First, the reservation value depends on mean-reversion speed θ: $\partial v^*/\partial\theta < 0$ when $v^* > \bar{v}$ and > 0 when $v^* < \bar{v}$. Second, the option value satisfies $\frac{\partial}{\partial v}[W(v) - v] < -1$ for $v \gg \bar{v}$ (agents rush to act at high payoffs), versus exactly -1 under i.i.d. search.

A.2 Matching microfoundation for Gaussian profits

This appendix provides a matching-theoretic microfoundation for the Gaussian matching efficiency function $m(n) = \exp(-\frac{\varphi}{2}(n - n_p)^2)$ stated in Assumption 2 of the main text (Gaussian scale efficiency).

Consider a market with n active firms. Each potential match between a firm and a trading partner has a quality θ drawn from a normal distribution $\theta \sim N(n_p, 1/\varphi)$. A firm operating at market thickness n captures matches with quality near n: specifically, matches within distance ε of n on the quality dimension. The density of good matches available to the firm is proportional to the normal density evaluated at n:

$$m(n) \propto \frac{1}{\sqrt{2\pi/\varphi}} \exp\Big(-\frac{\varphi}{2}(n - n_p)^2\Big).$$

This adapts the spatial-competition logic of Hotelling (1929) and Salop (1979) to market thickness: firms compete for matches along a continuum (the quality-density dimension) rather than along a geographic line or circle, and the normal distribution generates the Gaussian kernel. The connection to the equal-value structure of timing search runs through Burdett and Mortensen (1998), who carried the spatial-

equilibrium logic into wage posting; the present paper carries the same logic into the time dimension via the ironing condition. Absorbing the normalizing constant into π_0 yields $\pi(n) = \pi_0 \exp(-\frac{\varphi}{2}(n - n_p)^2)$.

The parameter φ inherits its interpretation from the variance of match qualities: $\varphi = 1/\mathrm{Var}(\theta)$. Industries with homogeneous match qualities (low variance, high φ) have a narrow peak and are sensitive to scale deviations. Industries with heterogeneous qualities (high variance, low φ) have a broad peak and are robust to deviations.

A.3 Derivation of the timing friction

This appendix derives the exponential-quadratic timing friction $\xi(\dot{n}) = e^{-\frac{\mu}{2}\dot{n}^2}$ as the continuous-time limit of proportional adjustment costs.

Discrete-time formulation Consider a discrete-time economy with period length $\Delta > 0$. In each period, effective output is reduced by a fraction proportional to the square of the adjustment speed:

$$y_t = \pi(n_t) \cdot \left[1 - \tfrac{\mu}{2}\left(\frac{n_{t+\Delta} - n_t}{\Delta}\right)^2 \Delta\right].$$

The adjustment cost is proportional to the square of the rate of change $(\Delta n/\Delta)^2$, scaled by the period length Δ. The parameter $\mu > 0$ governs the severity of the friction.

Continuous-time limit As $\Delta \to 0$, write $\dot{n} = \lim_{\Delta\to 0}(n_{t+\Delta} - n_t)/\Delta$ and note that $1 - x \approx e^{-x}$ for small x. The effective output becomes:

$$y(t) = \pi(n(t)) \cdot e^{-\frac{\mu}{2}\dot{n}(t)^2} = \pi(n(t)) \cdot \xi(\dot{n}(t)).$$

Robustness of the quadratic form Any symmetric friction $\xi(\dot{n})$ with $\xi(0) = 1$ and $\xi'(0) = 0$ admits the expansion $\ln \xi(\dot{n}) = -\frac{\mu}{2}\dot{n}^2 + O(\dot{n}^4)$, where $\mu = -\xi''(0)$. The leading-order dynamics—in particular $\omega = \sqrt{\varphi/\mu}$—depend only on μ, not on higher-order terms. The exponential-quadratic form is therefore canonical.

A.4 Detailed derivation of entry-matching micro-foundation

This appendix provides the detailed derivation of Assumption 3 in the main text (micro-foundation of the timing friction from entry-exit matching congestion).

Setup The matching function from the main text (§2.3) is $m(S, R) = S^{\alpha} R^{1-\alpha}$, where $S = M - n$ is the searcher pool and R is the stock of entry resources. The matching probability per searcher is $p(\theta_e) = \theta_e^{-(1-\alpha)}$ with $\theta_e = S/R$. The matching infrastructure R is tuned to clear the steady-state throughput $e_{ss} = \delta n_p$.

Steady state At $\dot{n} = 0$, the realized flow equals $e_{ss} = \delta n_p$, the infrastructure operates at its tuned capacity, and the matching probability equals $p_{ss} = p(\theta_e^{ss})$.

Bottleneck strain The gross entry flow is $e(t) = \dot{n}(t) + \delta n(t)$, with steady-state $e_{ss} = \delta n_p$, so the deviation of gross entry from the steady-state level is $e - e_{ss} = \dot{n} + \delta(n - n_p)$. Following the modeling convention adopted in the main text (Section 2.3), I attribute the slow-moving replacement component $\delta n(t)$ to a baseline capacity that tracks the prevailing population $n(t)$ and adjusts smoothly without bottleneck strain. The bottleneck-strain pipeline services only the net adjustment pressure $\dot{n}(t)$, which is the part of gross entry that exceeds the prevailing replacement rate. When $\dot{n} \neq 0$, this adjustment pressure deviates from zero in either direction. Rapid entry ($\dot{n} > 0$) strains the entry pipeline (permits, construction, specialist labor). Rapid net exit ($\dot{n} < 0$) strains the reallocation pipeline (resale markets, write-down procedures, workforce reassignment). Both reduce the matching probability per searcher below p_{ss}. I do not adopt a single-bottleneck specification in which one pipeline would service the full $|e - e_{ss}| = |\dot{n} + \delta(n - n_p)|$; the maintained model defines the bottleneck margin as net adjustment pressure $\dot{n}$ alone, in keeping with the modeling convention of Section 2.3 of the main text.

I represent this strain by a CES-like penalty that enters multiplicatively into the matching probability:

$$p(\theta_e;\, \dot{n}) = \theta_e^{-(1-\alpha)} \cdot \left[1 + \frac{\dot{n}^2}{2(\delta n_p)^2}\right]^{-(1-\alpha)/\alpha}. \tag{1}$$

The strain term depends on $\dot{n}^2$ rather than on signed $\dot{n}$, encoding the symmetry between entry and exit congestion. The $(\delta n_p)^2$ scale in the denominator reflects that

infrastructure capacity is calibrated to steady-state throughput: deviations small relative to δn_p are handled easily, while deviations approaching δn_p in magnitude strain the system to saturation.

What is assumed versus what is derived The specific CES functional form in (1) is a modeling choice: any smooth, symmetric strain penalty $g\big(\dot{n}^2/(\delta n_p)^2\big)$ with $g(0) = 0$ and $g'(0) = 1/2$ yields the same second-order behavior. The universality result in Online Appendix A.3 shows that *any* smooth symmetric friction ξ with $\xi(0) = 1$ and $\xi'(0) = 0$ admits the expansion $\ln \xi(\dot{n}) = -\frac{\mu}{2}\dot{n}^2 + O(\dot{n}^4)$ with $\mu = -\xi''(0)$; the second-order coefficient is therefore invariant to the particular smoothing chosen. What the specific form in (1) delivers is not the quadratic *shape* of the friction—that shape is universal—but the specific *scaling formula*

$$\mu = \frac{1-\alpha}{\alpha(\delta n_p)^2},$$

which pins the constant in terms of the matching elasticity α and the steady-state throughput δn_p. This scaling follows from two observations that hold for any reasonable smoothing: (i) the only natural scale for $\dot{n}$ is δn_p (steady-state throughput), so μ must be inversely proportional to $(\delta n_p)^2$ by dimensional reasoning; (ii) the matching elasticity α enters through the Cobb-Douglas term $\theta_e^{-(1-\alpha)}$, producing the $(1-\alpha)/\alpha$ factor regardless of which specific strain function is chosen. The CES form is a convenient representative of this equivalence class; alternatives (e.g., Gaussian strain $\exp[-\dot{n}^2/(2(\delta n_p)^2)]$, or quadratic strain $[1 - \dot{n}^2/(2(\delta n_p)^2)]$) yield the identical μ at second order.

Effective friction The effective output friction from the entry-replacement bottleneck is:

$$\ln \xi(\dot{n}) \equiv \ln p(\theta_e;\, \dot{n}) - \ln p(\theta_e^{ss}) = -\frac{1-\alpha}{\alpha} \ln\left[1 + \frac{\dot{n}^2}{2(\delta n_p)^2}\right].$$

Taylor expansion For small $|\dot{n}|/(\delta n_p)$, $\ln(1+x) = x - x^2/2 + \cdots$, and only the leading term contributes at second order in $\dot{n}$:

$$\ln \xi(\dot{n}) \approx -\frac{1-\alpha}{\alpha} \cdot \frac{\dot{n}^2}{2(\delta n_p)^2} + O(\dot{n}^4).$$

This is $-\frac{\mu}{2}\dot{n}^2$ with

$$\mu = \frac{1-\alpha}{\alpha(\delta n_p)^2} > 0.$$

Verification The friction ξ is symmetric ($\xi(\dot{n}) = \xi(-\dot{n})$), correctly signed ($\xi < 1$ for $\dot{n} \neq 0$), smooth (all derivatives exist at $\dot{n} = 0$), and matches the canonical quadratic form of Online Appendix A.3 to leading order. For $\alpha = 0.5$ (symmetric matching), $\mu = 1/(\delta n_p)^2$. For $\alpha = 0.7$ (searcher-weighted), $\mu = 3/(7(\delta n_p)^2) \approx 0.43/(\delta n_p)^2$, approximately 57% smaller—implying faster cycles in industries with higher searcher matching power.

B Proofs of main-text results

B.1 Spectral peak of the stochastic limit cycle

Proposition 3 (Stochastic limit cycle)**.**
Under small i.i.d. shocks $\tilde{\pi}(n,t) = \pi(n) + \sigma_\varepsilon \varepsilon_t$:

(i) The spectral density of $n(t)$ peaks at the structural frequency $\omega_0 = \sqrt{\varphi/\mu}$ in the undamped small-shock limit; with bottleneck damping $\eta = \chi/\mu > 0$, the observed PSD peak is $\omega_{PSD} = \sqrt{\varphi/\mu - \eta^2/2}$, equal to ω_0 up to an $O(\eta^2)$ correction (Proposition 4(iv)).

(ii) The peak frequency is determined by (φ, μ) at leading order and by the damping ratio η at second order, not by σ_ε.

(iii) Even i.i.d. shocks produce persistent cycles: the persistence is endogenous to the equilibrium structure.

Proof. Linearization. Under small shocks $\tilde{\pi}(n,t) = \pi(n) + \sigma_\varepsilon \varepsilon_t$ and Gaussian timing friction, the ironing condition with bottleneck damping (derived in Online Appendix B.2) linearized around $(n_p, 0)$ yields the damped stochastic oscillator

$$\ddot{n} + \eta\,\dot{n} + \omega_0^2\,(n - n_p) \;=\; \frac{\sigma_\varepsilon}{\mu}\,\varepsilon_t,$$

with $\omega_0 = \sqrt{\varphi/\mu}$ and $\eta = \chi/\mu$.

Spectral peak [claim (i)]. The linear filter from ε_t to $n(t) - n_p$ has transfer function

$$H(\nu) \;=\; \frac{1}{\omega_0^2 - \nu^2 + i\eta\nu},$$

so the stationary power spectral density is $S(\nu) = |H(\nu)|^2 S_\varepsilon(\nu)$. For white noise S_ε is constant in ν; maximizing $|H(\nu)|^2 = 1/[(\omega_0^2 - \nu^2)^2 + \eta^2\nu^2]$ in ν yields the peak at

$$\nu_{\text{peak}}^2 \;=\; \omega_0^2 - \eta^2/2.$$

In the undamped limit $\eta \to 0$, $\nu_{\text{peak}} \to \omega_0$ exactly. For $\eta \ll \omega_0$ (under-damped regime), ν_{peak} coincides with ω_0 up to a relative correction of $O(\eta^2/\omega_0^2)$, negligible at empirically relevant damping levels.

Parameter dependence [claim (ii)]. The peak location ν_{peak} is a function of $(\omega_0, \eta) = (\sqrt{\varphi/\mu}, \chi/\mu)$ alone. The shock variance σ_ε^2 scales the spectral density vertically (through S_ε) without shifting its argmax, so ν_{peak} does not depend on σ_ε.

Endogenous persistence [claim (iii)]. Even when S_ε is flat—i.i.d. shocks have no spectral concentration of their own—the resonant frequency response $|H(\nu)|^2$ concentrates output power near ν_{peak}. The persistence of cyclical fluctuations in $n(t)$ is therefore endogenous to the equilibrium structure (ω_0, η) rather than inherited from the shock process. ■

Remark (economic interpretation of the ironing condition). The ironing-condition energy identity $\frac{\mu}{2}\dot{n}^2 + \frac{\varphi}{2}(n - n_p)^2 = E$ of the main text decomposes into two economically interpretable pieces. The term $\frac{\mu}{2}\dot{n}^2$ is the per-firm flow cost of operating the matching kernel $\xi(\dot{n})$ at rate $\dot{n}$—the cost of keeping the entry rate at its current pace. The term $\frac{\varphi}{2}(n - n_p)^2$ is the per-firm profit shortfall from operating at scale n rather than at the optimum n_p. The ironing condition pins the sum of these two quantities at a constant level $E > 0$ along the equilibrium orbit: this is the equal-value level required by indifference across all entry dates. The four-phase cycle of Figure C.4 traces the periodic exchange between the two pieces: at $n = n_p$ the entire E sits in the entry-rate flow cost ($\dot{n}$ at maximum); at the turning points $n = n_p \pm A$ the entire E sits in the profit shortfall ($\dot{n} = 0$); in between, the two trade against each other while their sum remains pinned. The damped equilibrium adds the bottleneck dissipation channel $\chi\dot{n}^2$, which slowly erodes the equal-value level along the orbit and is balanced in the stationary equilibrium by injection from productivity shocks $\sigma_\varepsilon\varepsilon_t$.

Remark (persistent shocks). With persistent shocks $S_\varepsilon(\nu)$ is no longer flat, and the observed spectrum $S(\nu) = |H(\nu)|^2 S_\varepsilon(\nu)$ peaks where the product is maximized. Since $|H(\nu)|^2$ peaks at $\nu_{\text{peak}} = \sqrt{\omega_0^2 - \eta^2/2}$ while a persistent process (e.g., AR(1)) tilts S_ε toward low frequencies, the observed peak can shift slightly below ν_{peak}. The displacement is of order ρ/Q^2, where ρ is the shock autocorrelation and $Q = \omega_0/\eta$ is the quality factor of the transfer function. For sharp peaks ($Q \gg 1$), the displacement is negligible.

B.2 Stationary distribution of the damped stochastic oscillator

This appendix first derives the damped stochastic oscillator directly from the ironing condition with bottleneck dissipation, then derives the stationary amplitude distribution. The derivation balances the rate at which bottleneck dissipation erodes the equilibrium value level against the bottleneck's output-dissipation rate.

Proposition 4 (Amplitude selection)**.**
With bottleneck friction coefficient $\chi > 0$ (damping $\eta = \chi/\mu > 0$) and shocks $\sigma_\varepsilon > 0$:

(i) Without shocks ($\sigma_\varepsilon = 0$): orbits spiral inward to $(n_p, 0)$ with decay half-life $\ln 2 \cdot 2\mu/\chi$.

(ii) With shocks: the system has a unique stationary distribution with variance:

$$\mathbb{E}\big[(n - n_p)^2\big] = \frac{\sigma_\varepsilon^2}{2\,\eta\,\varphi\,\mu} = \frac{\sigma_\varepsilon^2}{2\,\chi\,\varphi}, \tag{2}$$

where the second equality uses $\eta = \chi/\mu$, so that the matching friction μ cancels.

(iii) The amplitude envelope $A = \sqrt{(n - n_p)^2 + (\dot{n}/\omega_0)^2}$ follows a Rayleigh distribution with scale $\sigma_x = \sigma_\varepsilon/\sqrt{2\chi\varphi}$, so that $\mathbb{E}[A^2] = 2\sigma_x^2 = \sigma_\varepsilon^2/(\chi\varphi)$.

(iv) The spectral peak frequency of the driven oscillator's stationary spectrum is $\omega_{peak} = \sqrt{\varphi/\mu - \eta^2/2}$, obtained by maximizing the squared frequency response $|H(\omega)|^2 = 1/[(\omega_0^2 - \omega^2)^2 + \eta^2\omega^2]$ over ω. (The homogeneous damped natural frequency $\sqrt{\varphi/\mu - \eta^2/4}$, at which the unforced solution oscillates, is a separate object.) For small η, both quantities are negligibly below $\sqrt{\varphi/\mu}$.

Proof. Frictionless equation from ironing. Under Gaussian profits (Assumption 2) and Gaussian friction (Assumption 3), the ironing condition (Proposition 1 of the main text) states $\pi(n)\xi(\dot{n}) = C$ along any equilibrium path. Linearizing around $(n_p, 0)$ and writing $x = n - n_p$:

$$\ln \pi(n_p) - \frac{\varphi}{2}x^2 - \frac{\mu}{2}\dot{n}^2 = \ln C.$$

Differentiating in time and cancelling the non-trivial factor $\dot{n} \neq 0$:

$$-\varphi\, x - \mu\, \ddot{n} = 0 \quad \Longleftrightarrow \quad \mu\, \ddot{n} + \varphi\, x = 0,$$

which is the law of motion of a frictionless oscillator with natural frequency $\omega_0 = \sqrt{\varphi/\mu}$, reproducing Theorem 1. The per-firm ironing-value functional

$$\mathcal{H} \equiv \tfrac{1}{2}\,\mu\,\dot{n}^2 + \tfrac{1}{2}\,\varphi\, x^2$$

is constant along the equilibrium orbit in the absence of dissipation, $\mathrm{d}\mathcal{H}/\mathrm{d}t = 0$ (this is the ironing-condition energy identity of the main text rewritten as a function of $(x, \dot{n})$).

Convex entry-replacement bottleneck. The entry-replacement pipeline is bottlenecked. Permits, specialized construction labor, site preparation for entrants, and reorganization services for replacement flow below attrition are all scarce relative to short bursts of flow, and the bottleneck strain rises with the squared departure of net adjustment pressure $\dot{n}$ from zero (Online Appendix A.4 derives this from microfoundations as the universal limit of congestion specifications). At the aggregate level I represent the strain by a Rayleigh dissipation function

$$R(\dot{n}) = \tfrac{1}{2}\,\chi\,\dot{n}^2, \qquad \chi > 0,$$

where χ is the bottleneck friction coefficient. Differentiating the dissipation function gives the dissipative force $-\partial R/\partial \dot{n} = -\chi\,\dot{n}$ in the equation of motion, with a rate of output dissipation $2R = \chi\,\dot{n}^2$ that erodes the ironing-value level along the orbit. I treat χ as a reduced-form damping primitive that selects the stationary cycle amplitude (Proposition 4 of the main text); I do not separately count $\chi\dot{n}^2$ as a contemporaneous output flow in the welfare ledger. The welfare cost of cycles in the welfare identity of the main text is captured by the displacement-curvature term $(\varphi/2)\mathbb{E}[x^2]$ and the firm-level friction term $(\mu/2)\mathbb{E}[\dot{n}^2]$ already; χ's role is to pin these losses at finite

stationary values through amplitude selection, not to add a third additive flow.

Primitive form: where χ comes from. The dissipation function $R(\dot{n}) = \frac{1}{2}\chi\dot{n}^2$ is not an ad hoc flow-level friction; it is the reduced form of a supplier-side optimization with two economic primitives. The supplier sector—permitting authorities, construction-labor markets, specialist equipment manufacturers, site preparation services—produces entry resources $R(t)$ at a smooth, convex cost $c(R)$, twice continuously differentiable around the steady-state resource level R_{ss} that services replacement at rate δn_p. Resources are consumed at two layers: a baseline layer that scales with the steady-state replacement flow δn, and a bottleneck layer that services net adjustment pressure $\dot{n}(t)$ above replacement through a linear technology,

$$R(t) - R_{ss} \;=\; r\,\dot{n}(t), \qquad r > 0,$$

where r is the *resource-flow linkage* (units of supplier-side resource flow per unit of net entry pressure). A second-order Taylor expansion of c around R_{ss} then gives

$$c\big(R_{ss} + r\dot{n}\big) - c(R_{ss}) - c'(R_{ss})\,r\dot{n} \;=\; \tfrac{1}{2}\,c_2\,r^2\,\dot{n}^2 \;+\; O(\dot{n}^3),$$

where $c_2 \equiv c''(R_{ss}) > 0$ is the *bottleneck curvature* (the supplier sector's cost convexity around steady-state flow). The constant $c(R_{ss})$ is absorbed into the ironing level C and does not affect dynamics. The linear term $c'(R_{ss})\,r\dot{n}$ averages to zero over a complete cycle—a closed orbit returns n to its initial value—so it neither dissipates output nor contributes to the per-firm welfare cost. Only the quadratic part dissipates, and matching to the rate $\chi\dot{n}^2$ in $R(\dot{n}) = \frac{1}{2}\chi\dot{n}^2$ identifies

$$\chi \;\equiv\; c_2\,r^2. \tag{3}$$

The bottleneck friction coefficient χ is therefore the product of two economic primitives: the supplier sector's cost curvature c_2 (a technology parameter of the supplier sector, in principle measurable from supplier-cost regressions) and the squared resource-flow linkage r (an input-requirement parameter of the entry production function, measurable from the resource intensity of new entry). Treating χ as primitive in Assumption 4 (bottleneck friction) of the main text is a deliberate aggregation choice: at the level of detail at which the body operates, only the product $c_2 r^2$ matters for cycle dynamics and welfare, and the closed-form results are unchanged by the disaggregation.

The disaggregation becomes operative when policy targets one primitive without the other—e.g., a permit-streamlining policy that lowers r without changing c_2, or a supplier-sector capacity expansion that lowers c_2 without changing r.

Value-flow balance derivation of the damped equation. Along any equilibrium path with bottleneck dissipation, the per-firm ironing-value functional $\mathcal{H}$ falls at exactly the rate at which the bottleneck consumes output:

$$\frac{\mathrm{d}\mathcal{H}}{\mathrm{d}t} = -\chi\,\dot{n}^2.$$

Computing the time derivative of $\mathcal{H}$ directly:

$$\frac{\mathrm{d}\mathcal{H}}{\mathrm{d}t} = \mu\,\dot{n}\,\ddot{n} + \varphi\,x\,\dot{n} = \dot{n}\,\big(\mu\,\ddot{n} + \varphi\,x\big).$$

Equating and cancelling $\dot{n}$ (for $\dot{n} \neq 0$):

$$\mu\,\ddot{n} + \varphi\,x = -\chi\,\dot{n}.$$

Rearranging:

$$\mu\,\ddot{n} + \chi\,\dot{n} + \varphi\,x = 0.$$

Dividing by μ and adding the stochastic forcing $\sigma_\varepsilon \varepsilon_t/\mu$ from Section 4 of the main text gives the damped stochastic oscillator

$$\ddot{n} + \eta\,\dot{n} + \omega_0^2\,x = \frac{\sigma_\varepsilon}{\mu}\,\varepsilon_t,$$

with $\omega_0 = \sqrt{\varphi/\mu}$ and

$$\eta = \frac{\chi}{\mu}.$$

Both signs are correct by construction: the restoring force $-\varphi x$ pulls the industry toward n_p, and the dissipative force $-\chi\dot{n}$ opposes motion. The damping rate η emerges endogenously from the ratio of the bottleneck friction coefficient χ (the strength of the bottleneck-strain mechanism) to the matching friction μ (how stiffly the ironing condition pins the motion). Higher friction dissipates output faster; higher matching friction slows both the restoring force and the dissipation by the same factor.

Noise convention and sampling-interval correction. The discrete-time shock ε_t with $\mathbb{E}[\varepsilon_t] = 0$ and $\mathbb{E}[\varepsilon_t^2] = 1$ is the per-period i.i.d. realization at sampling interval Δt.

In continuous-time terms, the equivalent forcing is $(\sigma_\varepsilon/\mu)\,\mathrm{d}W_t$ with $\mathbb{E}[(\mathrm{d}W_t)^2] = \mathrm{d}t$, related by $\sigma^2_{\varepsilon,\text{cont}} = \sigma^2_{\varepsilon,\text{disc}}/\Delta t$: the continuous-time shock variance is the discrete-per-period variance divided by the sampling interval. The closed-form stationary expressions $\sigma_x = \sigma_\varepsilon/\sqrt{2\chi\varphi}$ and $\mathbb{E}[\mathcal{L}] = \sigma^2_\varepsilon/(2\chi)$ derived below use the continuous-time form throughout, so cross-frequency calibrations require the conversion: a σ_ε measured at $\Delta t = 1$ month and a σ_ε measured at $\Delta t = 1$ year differ by a factor of $\sqrt{12}$ at the same underlying $\sigma_{\varepsilon,\text{cont}}$. All numerical welfare and amplitude calibrations in the body (Section 5.3 spectral test, Section 6.1 welfare numbers, Section 6.2 CHIPS counterfactual) use $\Delta t = 1$ month throughout for the FRED industrial-production series; the BDS-based per-industry welfare table in Online Appendix E.2 uses $\Delta t = 1$ year, with $\sigma^2_{\varepsilon,\text{ann}} = 12\,\sigma^2_{\varepsilon,\text{month}}$ applied so the implied χ is in common continuous-time units across the two series.

Important: σ_ε is the innovation of the model-implied second-order representation, not the raw amplitude. The linear time-aggregation $\sigma^2 \cdot \Delta t$ is the correct cross-frequency map only when the underlying object is white. The structural ε_t in equation (18) of the main text is i.i.d. by assumption, so for the structural innovation the aggregation is valid by construction. Section 5.4 and Online Appendix D.2 document that the *observed* per-industry series are non-AR(1) and that the BDS i.i.d. null is rejected for all eight industries even after AR(1) and AR(p)+GARCH prefiltering. This is exactly what the timing-search model predicts: equation (19) is a continuous-time second-order linear system, whose exact discretization is ARMA(2,1) rather than any finite AR(p), so generic reduced-form autoregressive filters provably fail to whiten the observed series. The whitening filter that does succeed by construction is the model-implied second-order representation itself.

The calibration that backs σ_ε out of $\sigma_x = \sigma_\varepsilon/\sqrt{2\chi\varphi}$ therefore uses the innovation of the fitted model-implied second-order representation: for each industry, the log-growth series is fitted to a discrete-time damped-oscillator state-space form (equivalently, an ARMA(2,1) with the parameter constraints implied by (19)), and the innovation standard deviation of that fitted representation is what enters as σ_ε. By construction, the residuals of the model-implied filter are i.i.d. at the sampling frequency, so the white-noise time-aggregation $\sigma^2_{\varepsilon,\text{cont}} = \sigma^2_{\varepsilon,\text{disc}}/\Delta t$ is valid on the calibrated innovation—and the fact that AR(p)+GARCH does not whiten the raw series (Appendix D.2) is consistent with the model, not in tension with this calibration.

Firewall: structural vs. reduced-form ω. The model-implied second-order fit (Ap-

pendix D.8) and the model-agnostic multitaper spectral peak (Table II) are distinct estimators of related but not identical objects: the multitaper estimator returns the dominant frequency of broadband power, while the model-implied fit returns the natural frequency of a constrained band-restricted second-order linear system. The two need not coincide outside the small-amplitude single-mode regime. They serve distinct, non-competing roles in the paper: the welfare calibration in this appendix uses only the model-implied fit, while the headline cross-industry slope test in Section 5.3 uses only the multitaper peak. There is no feedback between them.

Cross-frequency comparability. The monthly FRED series and the annual BDS series are estimated independently at their native sampling intervals ($\Delta t = 1$ month and $\Delta t = 1$ year respectively); the model-implied innovation is calibrated per-series from each. To put both calibrations in common continuous-time units I apply the conversion $\sigma^2_{\varepsilon,\text{cont}} = \sigma^2_{\varepsilon,\text{disc}}/\Delta t$ independently to each series. The relation $\sigma^2_{\varepsilon,\text{ann}} = 12\,\sigma^2_{\varepsilon,\text{month}}$ is the theoretical time-aggregation identity for a single underlying white process; it is *not* used here to transport a monthly σ_ε onto an annual-series welfare calculation. The BDS-based welfare numbers in Online Appendix E.2 are driven by each industry's own native-frequency (annual) calibrated innovation, converted to continuous-time units by dividing by $\Delta t = 1$ year; the monthly FRED-based numbers are driven by their own monthly calibrated innovation, converted by dividing by $\Delta t = 1$ month. The two welfare series are therefore both in continuous-time units of variance per year and are directly comparable, with no cross-series scaling.

Remark on the two entry-cost parameters. The bottleneck friction coefficient χ is structurally distinct from the per-firm sunk entry cost κ that appears in the free-entry condition $V(t) = V^{\text{search}}(t) + \kappa$ (Definition 1(ii) of the main text): κ is the dollar amount the marginal entrant pays at entry, while χ is the aggregate damping coefficient governing how strongly the bottleneck-strain mechanism opposes departures of net adjustment pressure $\dot{n}$ from zero. The two parameters have different units and different welfare implications. The welfare formula $\mathbb{E}[\mathcal{L}] = \sigma^2_\varepsilon/(2\chi)$ depends on χ alone; κ does not appear in it. Whether a real-world entry-cost policy moves κ, χ, or both is an institutional question that the model leaves open.

Setup. With the damped stochastic oscillator thus derived, the remainder of this appendix computes its stationary amplitude distribution.

Value-flow equation. Define the per-firm value functional $\mathcal{E} = \frac{1}{2}\dot{n}^2 + \frac{1}{2}\omega_0^2(n - n_p)^2$

(the rescaled ironing-value level). Then:

$$\mathrm{d}\mathcal{E} = -\eta\,\dot{n}^2\,\mathrm{d}t + \frac{\sigma_\varepsilon}{\mu}\,\dot{n}\,\mathrm{d}W_t + \frac{\sigma_\varepsilon^2}{2\mu^2}\,\mathrm{d}t.$$

Stationarity condition. In stationarity, $\mathbb{E}[\mathrm{d}\mathcal{E}] = 0$:

$$\eta\,\mathbb{E}[\dot{n}^2] = \frac{\sigma_\varepsilon^2}{2\mu^2}.$$

Equipartition. For the linear damped oscillator with white noise, the stationary distribution of $(n - n_p, \dot{n})$ is bivariate Gaussian. Equipartition gives:

$$\mathbb{E}[\dot{n}^2] = \omega_0^2\,\mathbb{E}[(n - n_p)^2].$$

The amplitude envelope satisfies $\mathbb{E}[A^2] = 2\mathbb{E}[(n - n_p)^2]$. Therefore:

$$\eta \cdot \frac{1}{2}\omega_0^2\,\mathbb{E}[A^2] = \frac{\sigma_\varepsilon^2}{2\mu^2}.$$

Solving:

$$\mathbb{E}[A^2] = \frac{\sigma_\varepsilon^2}{\mu^2\,\eta\,\omega_0^2} = \frac{\sigma_\varepsilon^2}{\mu\,\eta\,\varphi}.$$

Rayleigh distribution. The pair $(n - n_p, \dot{n}/\omega_0)$ is bivariate Gaussian with equal variances $\sigma_x^2 = \sigma_\varepsilon^2/(2\mu\eta\varphi)$. The envelope $A = \sqrt{(n - n_p)^2 + (\dot{n}/\omega_0)^2}$ therefore follows the Rayleigh distribution:

$$f(A) = \frac{A}{\sigma_x^2}\exp\!\left(-\frac{A^2}{2\sigma_x^2}\right), \qquad A \geq 0.$$

The mode is at σ_x and the mean is $\sigma_x\sqrt{\pi/2}$. Both scale linearly with σ_ε, confirming the linear relationship $\sigma_x \propto \sigma_\varepsilon$ (and equivalently $\sqrt{\mathbb{E}[A^2]} \propto \sigma_\varepsilon$). ■

B.3 Proof of Theorem 2 (Selection)

Theorem 2 of the body states that under $\sigma_\varepsilon, \chi > 0$ the stochastic dynamics of (9) admit a unique Markov stationary timing-search equilibrium (Definition 2), with a sharp deterministic limit as $\sigma_\varepsilon \downarrow 0$ and a small-noise/small-friction selection rule under joint scaling $\sigma_\varepsilon^2/\chi \to 2\bar{T}$. This appendix proves Theorem 2 for the linear-

Gaussian equilibrium implied by Assumptions 2–3 of the body—the object the entire empirical paper uses. A scoped conjecture on the non-Gaussian extension is recorded as Remark 1 at the end of Step 2. The proof has four steps: existence with explicit covariance, uniqueness under clause (iii), exponential mixing in total variation, and vanishing-noise selection.

Step 1 — Existence and explicit covariance Write the centred state vector $x_t = (n_t - n_p, \dot{n}_t)^\top \in \mathbb{R}^2$. Under the equilibrium policy e^*—pinned by clause (ii) of Definition 2 and by the linear form of the ironing condition (11)—equation (9) translates from the second-order scalar form to the equivalent first-order linear-Gaussian SDE

$$\mathrm{d}x_t = B\,x_t\,\mathrm{d}t + \Sigma_W\,\mathrm{d}W_t, \qquad B = \begin{pmatrix} 0 & 1 \\ -\varphi/\mu & -\chi/\mu \end{pmatrix}, \qquad \Sigma_W = \begin{pmatrix} 0 \\ \sigma_\varepsilon/\mu \end{pmatrix}. \tag{4}$$

The drift matrix B has trace $-\chi/\mu < 0$ and determinant $\varphi/\mu > 0$, so its eigenvalues have strictly negative real part, with explicit values

$$\lambda_\pm \;=\; -\frac{\chi}{2\mu} \;\pm\; i\sqrt{\frac{\varphi}{\mu} - \frac{\chi^2}{4\mu^2}}$$

in the empirically relevant under-damped regime $\chi^2 < 4\varphi\mu$ (the over-damped case is analogous and gives two negative real eigenvalues). By the standard Ornstein–Uhlenbeck representation (Itô's lemma applied to $e^{-Bt}x_t$), the law of x_t converges to a Gaussian invariant measure with covariance Σ^* solving the matrix equation

$$B\,\Sigma^* + \Sigma^* B^\top \;=\; -\,\Sigma_W\,\Sigma_W^\top \;=\; -\begin{pmatrix} 0 & 0 \\ 0 & \sigma_\varepsilon^2/\mu^2 \end{pmatrix}. \tag{5}$$

Writing $\Sigma^* = \left(\begin{smallmatrix} s_{11} & s_{12} \\ s_{12} & s_{22} \end{smallmatrix}\right)$ and expanding (5): the $(1,1)$ equation gives $s_{12} = 0$; the $(1,2)$ equation gives $s_{22} = (\varphi/\mu)\,s_{11}$; the $(2,2)$ equation gives $-2(\chi/\mu)\,s_{22} = -\sigma_\varepsilon^2/\mu^2$. Combining,

$$s_{11} \;=\; \frac{\sigma_\varepsilon^2}{2\chi\varphi}, \qquad s_{22} \;=\; \frac{\sigma_\varepsilon^2}{2\chi\mu},$$

i.e. $\Sigma^* = (\sigma_\varepsilon^2/2\chi\varphi)\,\mathrm{diag}(1, \varphi/\mu)$, as claimed in the body.

Step 2 — Uniqueness and verification of the equilibrium clauses In the linear-Gaussian system (4), uniqueness of the invariant law follows directly from the eigenvalues of B having strictly negative real part together with controllability of the pair (B, Σ_W) (Karatzas and Shreve, 1991, Thm. 5.7.7); see also Hasminskii (1980). Every initial law in $\mathcal{P}_2(\mathbb{R}^2)$ converges to a single Gaussian limit, so the family of invariant measures of (4) is a singleton.

We verify each clause of Definition 2 in turn. Clause (i) is satisfied by construction: the μ^* of Step 1 is the invariant law of (4) under the entry flow $e_t^* = \dot{n}_t + \delta n_t$ implied by aggregate consistency. For clause (ii), the linear-Gaussian structure pins V^* as the unique quadratic function of $(n - n_p, \dot{n})$ solving the continuous-time Bellman equation (10); existence is standard for linear-quadratic problems with the stability of B established in Step 1, and uniqueness up to an additive constant follows from the transversality requirement that $e^{-(r+\delta)t}\,\mathbb{E}[V^*(x_t)] \to 0$ as $t \to \infty$. For clause (iii), under the unique invariant law μ^* the marginal distribution of $(n_t, \dot{n}_t)$ equals μ^* at every t, so for any stopping time τ with $x_\tau \sim \mu^*$, the conditional expected option value $\mathbb{E}[V^*(n_\tau, \dot{n}_\tau)] = \mathbb{E}_{\mu^*}[V^*]$ is the same constant; clause (iii) is therefore automatically satisfied.

This proves Theorem 2 in full for the linear-Gaussian equilibrium under Assumptions 2–4—the regime that delivers the body's closed-form covariance, supports the entire empirical analysis, and to which the deterministic limit of Theorem 1 sharply reduces. The non-Gaussian extension is recorded as a scoped conjecture below.

Remark 1 (Non-Gaussian extension, conjecture)**.**
The argument above leans on Assumptions 2–3—Gaussian profit landscape and exponential-quadratic matching friction—so that the equation of motion is linear in $(n - n_p, \dot{n})$ and the invariant law is Gaussian. Outside that core, several modifications are conceivable: a profit landscape with multiple local maxima, a non-quadratic matching friction admitting cubic or higher-order terms in $\dot{n}$, or a bottleneck friction that responds nonlinearly to $|\dot{n}|$. In any such non-Gaussian extension, the diffusion may admit multiple stationary measures concentrated in distinct basins of the deterministic value landscape, and the linear-Gaussian uniqueness argument above no longer applies.

Conjecture. *Under any non-Gaussian extension for which (a) the deterministic value landscape has a unique global maximum at $(n_p, 0)$ and (b) the stochastic dynamics admit a stationary measure concentrated in its basin, clause (iii) of Definition 2 selects this measure as the unique Markov stationary timing-search equilibrium. The economic*

content is that any equilibrium supported in a different basin has strictly lower $\mathbb{E}_\mu[V^*]$*, so a stopping rule targeting the global-max basin would deliver a strict expected option-value gain, violating clause (iii).*

I do not attempt to prove the conjecture here. The standard regularity conditions of Villani (2009, Thm. 18) ensure that, under $\sigma_\varepsilon, \chi > 0$ *and a* C^2 *profit landscape with locally bounded curvature, each basin admits an invariant measure with exponentially mixing dynamics; this is the analytical machinery a proof would invoke. A full proof requires verifying clause (iii) on the multi-basin diffusion rather than asserting it. I leave the extension for separate work, and report Theorem 2 as a result on the linear-Gaussian equilibrium consistent with the rest of the body.*

Step 3 — Exponential mixing in total variation Because the eigenvalues of B have strictly negative real part (Step 1), with explicit values $\lambda_\pm = -\chi/(2\mu) \pm i\sqrt{\varphi/\mu - \chi^2/(4\mu^2)}$ in the under-damped regime $\chi^2 < 4\varphi\mu$ (the over-damped case is analogous), the conditional law of x_t given x_0 is Gaussian with mean $e^{Bt}x_0$ and covariance

$$\Sigma_t \;=\; \int_0^t e^{Bs}\,\Sigma_W\,\Sigma_W^\top\,e^{B^\top s}\,\mathrm{d}s \;\longrightarrow\; \Sigma^*.$$

Mean and covariance converge at exponential rate $\lambda = \chi/(2\mu)$, the absolute value of the real part of $\lambda_\pm$. Controllability of (B, Σ_W) is verified by the rank condition $\operatorname{rank}[\Sigma_W,\, B\Sigma_W] = 2$, and ensures that Σ_t is strictly positive definite for every $t > 0$. The transition kernel therefore admits a smooth density on $\mathbb{R}^2$ at every positive time. The total-variation bound between two Gaussians sharing the same covariance is $O(\|m_1 - m_2\|)$, and between two Gaussians with the same mean is $O(\|\Sigma_1 - \Sigma_2\|_F)$; combining,

$$\big\|\mathcal{L}(x_t \mid x_0) - \mu^*\big\|_{\mathrm{TV}} \;\le\; C\big(\|e^{Bt}x_0\| + \|\Sigma_t - \Sigma^*\|_F\big) \;\le\; C'\,e^{-\lambda t}(1 + \|x_0\|),$$

which integrates against any $\nu_0 \in \mathcal{P}_2(\mathbb{R}^2)$ to give the stated exponential bound. The non-Gaussian extension lies outside this argument; Remark 1 discusses the conjectured form.

Step 4 — Vanishing-noise selection Fix $\chi > 0$ and let $\sigma_\varepsilon \downarrow 0$. Then $\Sigma^* \to 0$ and $\mu^* \Rightarrow \delta_{(n_p,0)}$ weakly—the point mass at the deterministic steady state of Theorem 1. This is the standard small-noise limit of Freidlin and Wentzell (2012): exit times from

any neighbourhood of $(n_p, 0)$ diverge exponentially in $1/\sigma_\varepsilon^2$, so μ^*-mass concentrates on the steady state alone.

Now let $\sigma_\varepsilon, \chi \downarrow 0$ jointly along $\sigma_\varepsilon^2/\chi \to 2\bar{T}$ for some $\bar{T} > 0$. The covariance rescales as $\Sigma^* \to (\bar{T}/\varphi)\,\mathrm{diag}(1, \varphi/\mu)$, a non-degenerate Gaussian whose expected per-firm welfare cost $\frac{1}{2}\varphi s_{11} + \frac{1}{2}\mu s_{22}$ equals $\bar{T}$ by direct substitution. Because the Gaussian's covariance is proportional to the inverse Hessian of the quadratic value-deviation function at its maximizer, this Gaussian is the *unique* stationary distribution of (9) with expected welfare cost $\bar{T}$. The selection is sharp: any other scaling of $(\sigma_\varepsilon, \chi) \downarrow (0, 0)$ either collapses Σ^* to zero or sends it to infinity, neither of which is a stationary equilibrium in the sense of Definition 2. □

B.4 General hump-shaped profits

Proposition 5 (General hump-shaped profits)**.**
Under any C^2 profit function $\pi(n)$ with $\pi'(n_p) = 0$ and $\pi''(n_p) < 0$, and timing friction $\xi(\dot{n}) = e^{-\frac{\mu}{2}\dot{n}^2}$, the ironing condition $\ln \pi(n) - \frac{\mu}{2}\dot{n}^2 = E$ admits periodic orbits with frequency near n_p given by $\omega = \sqrt{|f'(n_p)|/\mu} + O(A^2)$, where $f'(n_p) = \pi''(n_p)/\pi(n_p) < 0$. For the Gaussian specification, $|f'(n_p)| = \varphi$ exactly. A numerical check across 8 smooth exponential-family hump-shaped profit specifications shows the Gaussian-based prediction $T_0 = 2\pi\sqrt{\mu/\varphi}$ stays within 1.6% of the exact orbit-integrated period at $A/n_p = 0.30$ (Online Appendix C.2).

Proof. Let $\pi(n)$ be a C^2 function with $\pi(n) > 0$ for n in a neighborhood of n_p, $\pi'(n_p) = 0$, and $\pi''(n_p) < 0$. The ironing condition gives:

$$\ln \pi(n) - \frac{\mu}{2}\dot{n}^2 = E.$$

Define the profit-curvature kernel $U(n) = -\frac{1}{\mu}\ln \pi(n)$, which encodes how the profit landscape confines the industry near optimal scale. Since $\pi'(n_p) = 0$ and $\pi''(n_p) < 0$, $U'(n_p) = 0$ and $U''(n_p) = -\pi''(n_p)/(\mu\pi(n_p)) > 0$, so n_p is a local minimum of U. This becomes:

$$\frac{1}{2}\dot{n}^2 + U(n) = -\frac{E}{\mu} \equiv \mathcal{E}.$$

Economically, this says that the sum of the profit-landscape cost $U(n)$ and the adjustment cost $\frac{1}{2}\dot{n}^2$ is constant along the equilibrium path. The economy oscillates around n_p because deviations from optimal scale are offset by adjustment dynamics.

For $\mathcal{E}$ slightly above $U(n_p)$, the oscillations have small amplitude. The frequency of small oscillations is:

$$\omega = \sqrt{U''(n_p)} = \sqrt{\frac{-\pi''(n_p)}{\mu\,\pi(n_p)}} = \sqrt{\frac{|f'(n_p)|}{\mu}},$$

where $f'(n_p) = [\pi''/\pi - (\pi'/\pi)^2]|_{n_p} = \pi''(n_p)/\pi(n_p)$ since $\pi'(n_p) = 0$.

For finite amplitude A, the period of oscillation under a general profit landscape is:

$$T(A) = \sqrt{2}\int_{n_-}^{n_+} \frac{\mathrm{d}n}{\sqrt{\mathcal{E} - U(n)}},$$

where $n_\pm$ are the turning points. Expanding $U(n)$ to fourth order around n_p:

$$U(n) = U(n_p) + \frac{1}{2}U''(n_p)(n-n_p)^2 + \frac{1}{6}U'''(n_p)(n-n_p)^3 + \frac{1}{24}U^{(4)}(n_p)(n-n_p)^4 + \cdots$$

Standard perturbation theory for nonlinear oscillators gives:

$$\omega(A) = \omega_0 + O(A^2),$$

where $\omega_0 = \sqrt{U''(n_p)} = \sqrt{|f'(n_p)|/\mu}$.

For the Gaussian specification, $U(n) = \frac{\varphi}{2\mu}(n-n_p)^2 + \text{const}$ exactly (all higher-order terms vanish), so $\omega = \omega_0$ exactly for all A. For $\pi(n) = n^\alpha(a - bn)$, the cubic and quartic corrections are nonzero, producing amplitude-dependent corrections to the frequency. ■

B.5 Entry at all dates: verification of the regularity condition

This appendix verifies the all-entry regularity condition used in Theorem 1 of the main text—namely, that entry occurs at every date along the deterministic equilibrium orbit.

Proposition 6 (Joint regularity bound on cycle amplitude)**.**
The timing search equilibrium of Theorem 1 satisfies the all-dates regularity condition—a positive searcher pool $S(t) > 0$ and a positive entry flow $e(t) = \dot{n}(t) + \delta n(t) > 0$ at

every date—if and only if the cycle amplitude satisfies the joint upper bound

$$A \;\leq\; \min\left\{ \frac{\delta n_p}{\sqrt{\omega^2+\delta^2}}\,,\; M - n_p - \varepsilon \right\}, \tag{6}$$

for any $\varepsilon > 0$. The first term in the minimum (the binding component for typical M) is the entry-flow bound: the steady-state exit flow δn_p must exceed the maximum amplitude of net flow oscillation. The second term is the searcher-pool bound: the active population must remain strictly below the total population M over the cycle.

Proof. Along the equilibrium path, $n(t) = n_p + A\cos(\omega t + \phi)$, so $S(t) = M - n(t) \geq M - n_p - A > 0$ iff $A < M - n_p$, which the second term of (6) ensures for any $\varepsilon > 0$.

The entry flow is $e(t) = \dot{n}(t) + \delta n(t) = -A\omega\sin(\omega t+\phi) + \delta(n_p + A\cos(\omega t+\phi))$. The non-constant component $-A\omega\sin(\cdot) + \delta A\cos(\cdot)$ has maximum modulus $A\sqrt{\omega^2+\delta^2}$, so $e(t) > 0$ for all t iff $\delta n_p > A\sqrt{\omega^2+\delta^2}$, i.e., iff $A < \delta n_p/\sqrt{\omega^2+\delta^2}$, which is the first term of (6).

The joint condition $A \leq \min\{\cdot,\cdot\}$ is therefore necessary and sufficient. ■

Empirical scope: closed-form Theorem 1 vs. Proposition 4 spectral peak. For manufacturing industries with $\delta_i \in [0.065, 0.090]$ and ω_i in the business-cycle band ($\omega_i \in [1.3, 2.1]$ in radians/year), the first term of (6) gives $A_i^{\max}/n_{p,i} \in [0.031, 0.069]$: the closed-form exact-harmonic Theorem 1 is a *small-amplitude benchmark* valid for cycles up to roughly 3–7% of steady-state scale. This is the natural scope of an analytical theorem and is not the empirical target. The empirical analysis in Section 5 (spectral tests, cross-industry slope, IV) targets the stochastic damped system of Proposition 4, whose spectral peak inherits the closed-form natural frequency $\omega_0 = \sqrt{\varphi/\mu}$ up to an $O(\eta^2)$ correction at empirically relevant damping and amplitudes; that peak is the object recovered by multitaper, Burg AR(12), and the 2SLS, all of which are valid outside the small-amplitude regime. Industries with large investment swings—e.g., manufacturing structures during the Great Depression episode (Figure 5a) or oil/mining during the 1979 crisis (Figure 5b)—sit well outside the closed-form regime, and the analysis of those impulse responses leans on the stochastic damped system's spectral peak (Proposition 4) and the isochrony of damped oscillation (Online Appendix C.1), not on Theorem 1's exact orbit. The closed-form theorem and the empirical spectral object are therefore separate but consistent: the theorem pins the small-amplitude natural frequency in closed form; the stochastic damped system

inherits that frequency at empirically observed amplitudes.

B.6 Frequency correction and cycle asymmetry

Proposition 7 (Frequency correction at finite amplitude)**.**
Under any C^2 profit function $\pi(n)$ with $\pi'(n_p) = 0$ and $\pi''(n_p) < 0$, and timing friction $\xi(\dot{n}) = e^{-\frac{\mu}{2}\dot{n}^2}$, the closed-form frequency $\omega_0 = \sqrt{|f'(n_p)|/\mu}$ admits the finite-amplitude expansion

$$\omega(A) = \omega_0\big[1 + c_4 A^2 + O(A^4)\big]\,,$$

where $c_4 = \frac{\gamma}{16\omega_0^2} - \frac{5\beta^2}{48\omega_0^4}$ is a profit-curvature functional with $\beta = U'''(0)$ and $\gamma = U^{(4)}(0)$ for $U(x) = -\mu^{-1}\ln\pi(n_p + x)$. For Gaussian profits $\beta = \gamma = 0$ and $\omega(A) = \omega_0$ for all A (exact isochrony as the $c_4 = 0$ knife-edge); for the quartic perturbation $\pi(n) = \pi_0 e^{-\frac{\varphi}{2}x^2 - a_4 x^4}$, $c_4 = 3a_4/(2\varphi)$, recovering the formula $\omega(A) = \omega_0(1 + 3a_4 A^2/(2\varphi))$.

Proof. Setup. Consider the oscillator $\ddot{x} + U'(x) = 0$, where $x = n - n_p$ and $U(x) = U_0 + \frac{1}{2}\omega_0^2 x^2 + \frac{1}{6}\beta x^3 + \frac{1}{24}\gamma x^4 + \cdots$, with $\omega_0 = \sqrt{U''(0)}$, $\beta = U'''(0)$, $\gamma = U^{(4)}(0)$.

Perturbative expansion. Seek a periodic solution:

$$x(t) = A\cos(\omega t) + A^2 x_2(t) + A^3 x_3(t) + \cdots\,,$$

$$\omega = \omega_0 + A^2\omega_2 + O(A^4).$$

(Odd powers of A vanish by symmetry when $\beta = 0$.)

Order A^2. Substituting into the equation of motion and collecting $O(A^2)$ terms:

$$\ddot{x}_2 + \omega_0^2 x_2 = -\frac{\beta}{2}\cos^2(\omega_0 t) = -\frac{\beta}{4}[1 + \cos(2\omega_0 t)].$$

The particular solution is:

$$x_2(t) = -\frac{\beta}{4\omega_0^2} + \frac{\beta}{12\omega_0^2}\cos(2\omega_0 t).$$

Order A^3 (resonance condition). At $O(A^3)$, the equation becomes:

$$\ddot{x}_3 + \omega_0^2 x_3 = \left[2\omega_0\omega_2 - \frac{\gamma}{8} + \frac{5\beta^2}{24\omega_0^2}\right]\cos(\omega_0 t) + \cdots$$

Eliminating the resonant term at frequency ω_0:

$$\omega_2 = \frac{1}{2\omega_0}\left[\frac{\gamma}{8} - \frac{5\beta^2}{24\omega_0^2}\right].$$

Result. The corrected frequency is:

$$\omega(A) = \omega_0\left[1 + \left(\frac{\gamma}{16\omega_0^2} - \frac{5\beta^2}{48\omega_0^4}\right)A^2 + O(A^4)\right].$$

For the Gaussian profit: $U(x) = \frac{\varphi}{2\mu}x^2$ exactly (no higher terms), so $\beta = \gamma = 0$ and $\omega(A) = \omega_0$ for all A (exact isochrony).

For the quartic perturbation $\pi(n) = \pi_0 e^{-\frac{\varphi}{2}x^2 - a_4 x^4}$: $U(x) = \frac{\varphi}{2\mu}x^2 + \frac{a_4}{\mu}x^4$, so $\beta = 0$ and $\gamma = 24a_4/\mu$. Then $\omega_2 = \frac{3a_4}{2\mu\omega_0}$, giving:

$$\omega(A) = \omega_0\left(1 + \frac{3a_4}{2\varphi}A^2\right),$$

where $\omega_0^2 = \varphi/\mu$, confirming the formula used in the numerical experiments. ■

Proposition 8 (Cycle asymmetry under cubic profit curvature)**.**
When $\pi'''(n_p) \neq 0$, the orbit is asymmetric: the leading-order excess time spent above versus below n_p is $\mathcal{A} = \pi'''(n_p)/[\pi\,|\pi''(n_p)|]\cdot A + O(A^2)$. When $\pi'''(n_p) < 0$ (profit falls faster on the congestion side), $\mathcal{A} < 0$ and the economy spends more time below n_p, producing slow expansions and sharp contractions.

Proof. When $\beta = U'''(0) \neq 0$, the $O(A^2)$ correction $x_2(t)$ includes a constant shift $-\beta/(4\omega_0^2)$ and a second-harmonic term. The time-averaged position deviation from n_p is therefore $\langle x\rangle = -A^2\beta/(4\omega_0^2)$, which displaces the orbit and makes it spend unequal time above and below n_p. To leading order in A, write $x(t) = A\cos(\omega_0 t) + \langle x\rangle$ and set $\epsilon = -\langle x\rangle/A = A\beta/(4\omega_0^2)$. The fraction of the period with $x(t) > 0$ is $\arccos(\epsilon)/\pi \approx 1/2 - \epsilon/\pi$ for small ϵ, so the time-fraction asymmetry is

$$\begin{aligned}\mathcal{A} &\equiv \frac{t_{\text{above}} - t_{\text{below}}}{t_{\text{below}}} \\ &= -\frac{4\epsilon}{\pi} + O(\epsilon^2) = -\frac{\beta}{\pi\,\omega_0^2}\,A + O(A^2)\end{aligned}$$

(positive sign when the time-averaged position is above n_p, i.e., when $\beta < 0$). Express-

ing β through the profit function yields

$$U'''(0) = -\frac{\pi'''(n_p)\pi(n_p) - 3\pi''(n_p)\pi'(n_p)}{\mu\pi(n_p)^2}.$$

Since $\pi'(n_p) = 0$, this simplifies to

$$\beta = -\frac{\pi'''(n_p)}{\mu\pi(n_p)}, \qquad \omega_0^2 = \frac{|\pi''(n_p)|}{\mu\pi(n_p)}.$$

Therefore:

$$\mathcal{A} = \frac{\pi'''(n_p)}{\pi\,|\pi''(n_p)|}\,A + O(A^2).$$

When $\pi'''(n_p) < 0$ (profit falls faster on the congestion side), $\mathcal{A} < 0$: the economy spends more time below n_p, producing slow expansions and sharp contractions. ■

B.7 Equilibrium verification

This appendix verifies that the path constructed in Theorem 1 satisfies all five conditions of the timing search equilibrium (Definition 1).

Entry policy and aggregate consistency (iv) The entry policy implied by the equilibrium path is $e(t) = \dot{n}(t) + \delta n(t)$. Using $n(t) = n_p + A\cos(\omega t + \phi)$:

$$e(t) = -A\omega\sin(\omega t + \phi) + \delta(n_p + A\cos(\omega t + \phi)).$$

This satisfies $\dot{n} = e - \delta n$ by construction.

Entry non-negativity For $e(t) \geq 0$ at all dates, the condition $\delta n_p > A\sqrt{\omega^2 + \delta^2}$ must hold, i.e., the steady-state exit flow must exceed the maximum amplitude of the net flow. This holds whenever the cycle amplitude is moderate relative to steady-state scale: $A < \delta n_p/\sqrt{\omega^2 + \delta^2}$.

Sufficiency of the ironing condition (i, iii) The ironing condition gives $\pi(n(t))\xi(\dot{n}(t)) = C$ for all t. Substituting this constant into the value function

$V(\tau) = \int_\tau^\infty e^{-(r+\delta)(t-\tau)}\pi(n(t))\xi(\dot{n}(t))\,\mathrm{d}t$ from the main text yields

$$V(\tau) = \int_\tau^\infty e^{-(r+\delta)(t-\tau)}\,C\,\mathrm{d}t = \frac{C}{r+\delta} \equiv V^*$$

for all τ. Since $V(\tau)$ is the same at every date, each agent's entry date is optimal (condition (i)) and no agent can gain by retiming (condition (iii)). The ironing condition is therefore sufficient, not just necessary, for individual optimality.

Temporal free entry (ii) Along the equilibrium path, $V(\tau) = V^* = C/(r+\delta)$ for all τ. Free entry requires $V(\tau) = V^{\text{search}}(\tau) + \kappa$, which pins $V^{\text{search}} = V^* - \kappa$ at all dates. Since V^* is constant, this is satisfied identically.

Feasibility (v) The maximum of $n(t)$ is $n_p + A$. Feasibility requires $n_p + A \leq M$, i.e., the total population must exceed the peak number of active firms. With A moderate and M large, this holds.

C Numerical robustness

C.1 Additional simulation results

This appendix provides computational verification of the timing search model, including the spectral density comparison referenced in the main text. I simulate the stochastic system $(n, \dot{n})$ via Euler–Maruyama discretization with illustrative parameters $\varphi = 4$, $\mu = 1$, $\sigma_\varepsilon = 0.05$, $n_p = 1$ (theoretical prediction: $\omega_0 = 2$, $T^* = \pi \approx 3.14$ time units), chosen to produce a clean theoretical prediction rather than to match a specific industry. The paper's empirical content comes from Section 5 of the main text, where the cross-industry predictions are tested using industry-specific proxies.

Spectral density Figure C.1 plots the power spectral density (Welch's method) of the simulated model against an AR(1) benchmark. The timing search model concentrates spectral mass in a narrow band around $\omega_0 = 2.0$, matching the structural prediction up to the small $O(\eta^2)$ damping shift. The peak rises four orders of magnitude above the surrounding frequencies: the scale–congestion trade-off selectively amplifies fluctuations near ω_0 and attenuates those at other frequencies. The AR(1) benchmark

produces a featureless, monotonically decaying spectrum—the signature of dynamics inherited entirely from the shock process. This confirms Proposition 3 of the main text: the spectral peak is a *structural* object, pinned by (φ, μ) at leading order and invariant to σ_ε.

Figure C.1: Spectral density: stochastic timing search vs. AR(1)

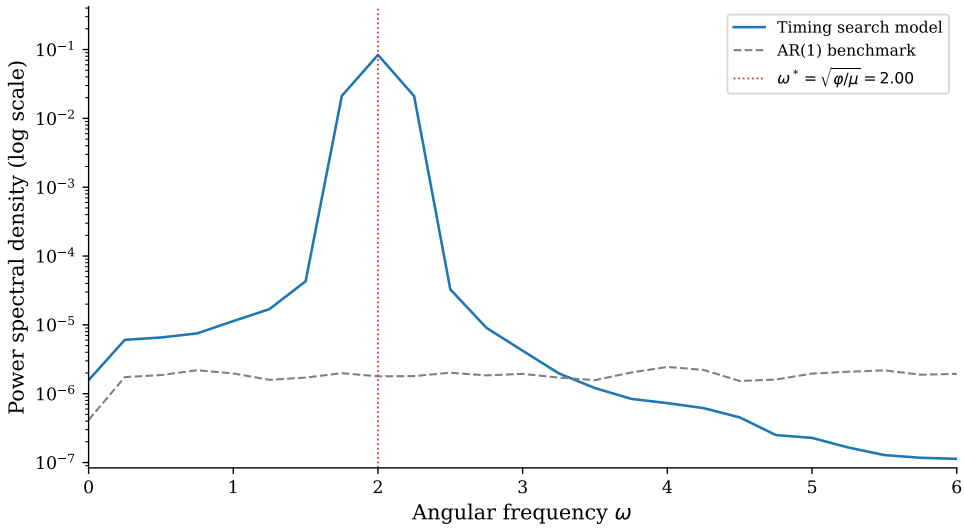

Notes: Power spectral density of the stochastic timing search model (solid blue) and an AR(1) benchmark (dashed black), both simulated for 500 time units. The red dotted line marks the structural frequency $\omega_0 = \sqrt{\varphi/\mu} = 2.0$. The model's spectral peak coincides with ω_0 up to the small $O(\eta^2)$ damping correction $\omega_{\text{PSD}} = \sqrt{\omega_0^2 - \eta^2/2}$. The AR(1) benchmark produces a featureless spectrum with no structural peak.

Damped impulse response Figure C.2 illustrates the impulse-response behaviour of the main-text damped equation $\ddot{n}+\eta\dot{n}+(\varphi/\mu)(n-n_p) = (\sigma_\varepsilon/\mu)\varepsilon_t$ in the deterministic-but-damped case ($\sigma_\varepsilon = 0$, $\eta > 0$, $x(0) = A_0 \neq 0$), the case the empirical echo analysis examines in manufacturing investment. Three damping rates $\eta \in \{0.05, 0.20, 0.45\}$ are plotted with fixed (φ, μ) so the natural frequency $\omega_0 = \sqrt{\varphi/\mu} = 1$ is common. Each trajectory's envelope decays exponentially at rate $\eta/2$, but zero crossings occur at nearly identical times: the pitch is preserved while the volume fades. This decoupling of declining amplitude from preserved period is a distinctive feature of the timing-search equilibrium and contrasts with linear models such as AR(1), where the decay rate and period are mechanically linked.

Figure C.2: Damped impulse response of the timing-search equilibrium

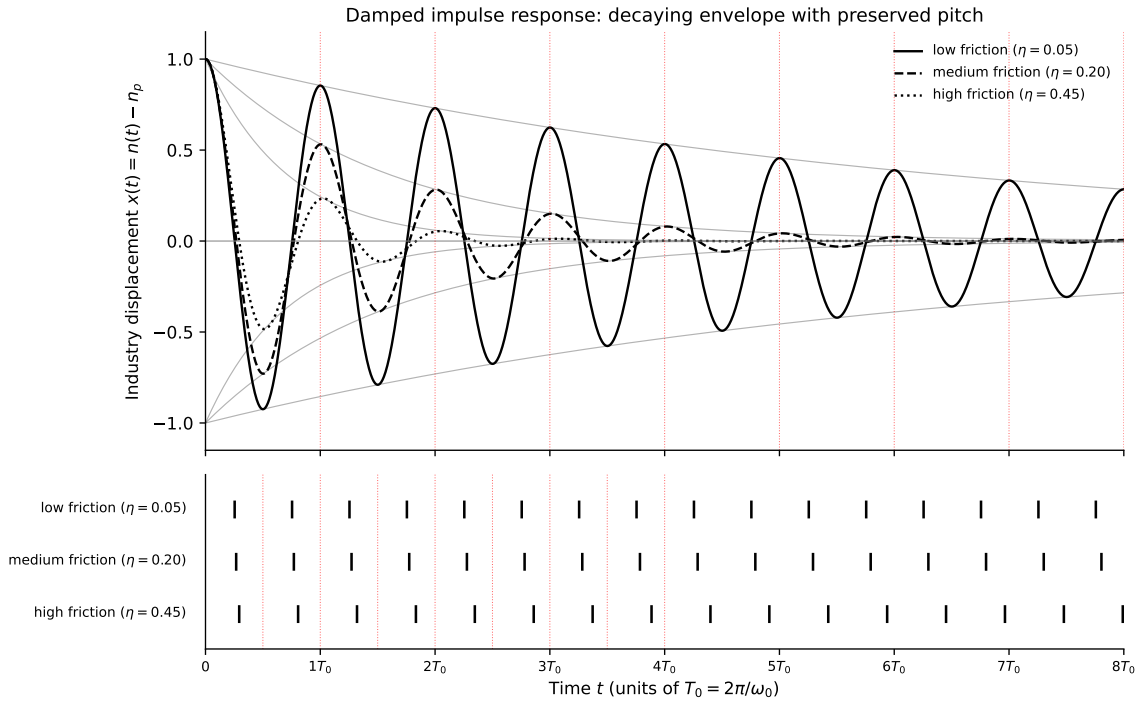

Notes: The damped harmonic oscillator $\ddot{x} + \eta\,\dot{x} + (\varphi/\mu)\,x = 0$ with $x(0) = A_0$, $\dot{x}(0) = 0$, and fixed natural frequency $\omega_0 = \sqrt{\varphi/\mu} = 1$. Three damping rates $\eta \in \{0.05, 0.20, 0.45\}$ are plotted. Top panel: trajectories with the exponential envelope $A_0 e^{-\eta t/2}$ shown in grey; the dotted red grid marks integer multiples of $T_0 = 2\pi/\omega_0$. Bottom panel: zero crossings of each trajectory, showing that the half-period marker (red) approximately coincides with each crossing for small damping (the exact zero-crossing times depend on η and align with $T_0/2$ markers only to leading order). Higher friction damps the envelope faster but leaves the pitch ω_0 essentially unchanged.

Stationary amplitude distribution Figure C.3 verifies the quantitative content of the amplitude selection result numerically. Panel (a) overlays simulated histograms of the amplitude envelope $A(t) = \sqrt{(n(t) - n_p)^2 + (\dot{n}(t)/\omega_0)^2}$ on the theoretical Rayleigh density with scale $\sigma_x = \sigma_\varepsilon/\sqrt{2\chi\varphi}$ for several shock volatilities; the simulated and theoretical densities coincide closely across the range. Panel (b) tracks the stationary standard deviation of $(n - n_p)$ as σ_ε varies, recovering the linear relationship $\sigma_x \propto \sigma_\varepsilon$.

BDS test for nonlinear dependence The BDS test (Brock, Dechert, and Scheinkman, 1996) examines whether AR(1)-filtered residuals contain nonlinear serial dependence. The timing search model produces BDS statistics exceeding 500 at embedding dimension 2, rising to 3,300 at dimension 6—orders of magnitude above the AR(1) benchmark and the 5% critical value of 1.96. The escalation with embedding

Figure C.3: Stationary amplitude distribution

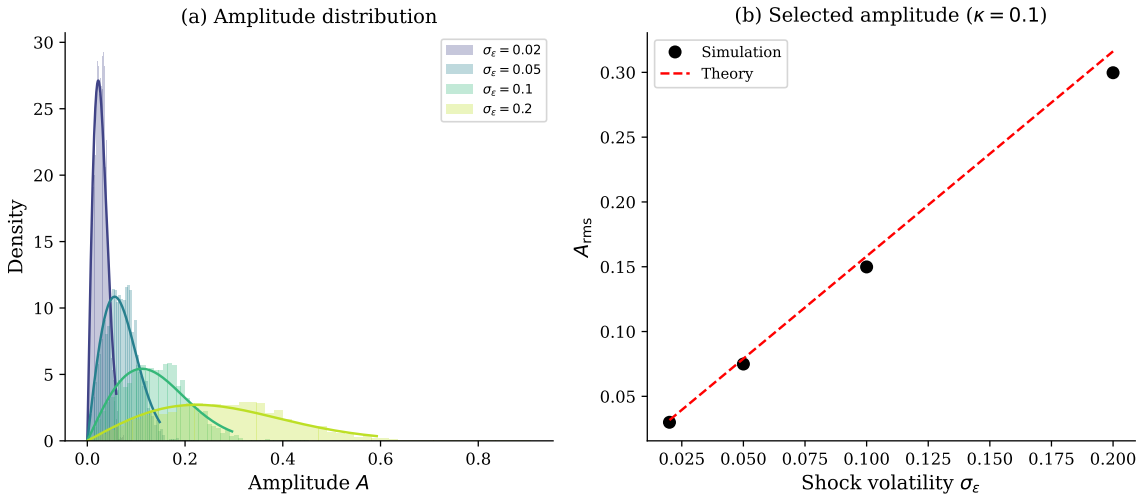

Notes: Panel (a): histogram of the amplitude envelope $A = \sqrt{(n - n_p)^2 + (\dot{n}/\omega_0)^2}$ from simulations with $\chi = 0.1$ and varying shock volatility σ_ε, with theoretical Rayleigh density (scale σ_x) overlaid. Panel (b): stationary standard deviation of $(n - n_p)$ vs. shock volatility, confirming the linear relationship $\sigma_x \propto \sigma_\varepsilon$.

dimension reflects the deterministic skeleton underlying the stochastic dynamics: the ironing condition confines the economy to a two-dimensional manifold in $(n, \dot{n})$ space, and higher-dimensional embeddings detect this geometric structure with increasing power.

C.2 Beyond the Gaussian: robustness display

This appendix documents the numerical check of the Gaussian-frequency formula across non-Gaussian profit specifications and illustrates the cycle-asymmetry prediction.

Worst-case frequency error A direct numerical check confirms that the Gaussian approximation is quantitatively tight. Across a library of 8 smooth exponential-family hump-shaped profit specifications—the Gaussian with $\varphi \in \{1, 4, 9\}$ together with quartic and cubic perturbations up to ± 0.5 of the curvature parameter—the worst-case frequency error from using $\omega_0 = \sqrt{\varphi/\mu}$ in place of the exact orbit-integrated period is 1.6% at $A/n_p = 0.30$.

Table C.1: Worst-case frequency error from the Gaussian approximation

Amplitude A/n_p	0.05	0.10	0.15	0.20	0.25	0.30
Worst-case error (paper's class)	0.05%	0.19%	0.42%	0.74%	1.15%	1.64%

Notes: Worst-case frequency error across 8 smooth exponential-family hump-shaped profit specifications (Gaussian at $\varphi \in \{1, 4, 9\}$; quartic perturbations $a_4 \in \{-0.2, +0.2, +0.5\}$; cubic/skew perturbations $a_3 \in \{-0.3, +0.3\}$). Each row reports the maximum of $|T_{\text{exact}} - T_0|/T_0$ where T_{exact} is obtained by numerically integrating the ironing orbit and $T_0 = 2\pi\sqrt{\mu/\varphi}$ is the Gaussian-based prediction. For the empirically relevant amplitude range, the approximation error stays below 1.64%.

Asymmetric cycles Figure C.4 illustrates the contrast between symmetric and asymmetric profits. Under symmetric (Gaussian) profits, peaks and troughs are equal in magnitude. Under asymmetric profits with $\pi'''(n_p) < 0$, booms overshoot while busts are shallower, matching the well-known empirical asymmetry. The degree of asymmetry is pinned by the ratio $\pi'''(n_p)/|\pi''(n_p)|$.

Figure C.4: Asymmetric cycles under skewed profits

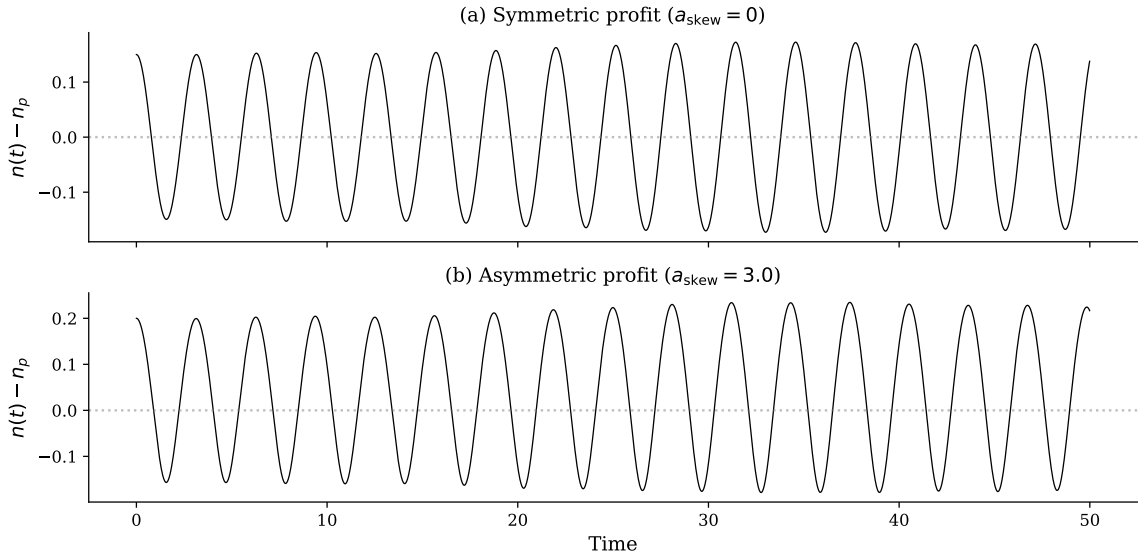

Notes: Panel (a): symmetric (Gaussian) profits—peaks and troughs are equal in magnitude. Panel (b): asymmetric profits ($\pi'''(n_p) < 0$, steeper congestion side). Booms overshoot ($n - n_p \approx 0.20$) while busts are shallower ($n - n_p \approx -0.15$). Both panels share the same initial condition and frequency.

Quartic and skewed perturbations Figure C.5 quantifies the Gaussian approximation error across four exercises. Panel (a) plots the spectral peak frequency obtained by simulating the equilibrium under quartic-perturbed profits

$\pi(n) = \pi_0 \exp[-(\varphi/2)x^2 - a_4 x^4]$ for a range of a_4 values, and compares it to the Gaussian benchmark $\omega_0 = 2.0$. Panel (b) reports the same comparison as a percentage deviation: the error stays below 5% for $a_4 \leq 2$, well within the empirically relevant range. Panel (c) traces the analytical nonlinear frequency correction $\omega(A) = \omega_0(1 + 3a_4 A^2/(2\varphi))$ from Proposition 7 against simulated frequencies as the amplitude A increases; the analytical curve overlays the simulation points almost exactly. Panel (d): as the skewness coefficient a_{skew} rises, the fractional difference in time spent above versus below n_p grows monotonically, in line with the asymmetry prediction.

D Empirical detail

D.1 Broad-sector baseline regression (N=7)

This appendix documents the proxy construction, regression specification, and robustness checks for the $N = 7$ broad-sector baseline regression summarized in the main text.

The model's quantitative prediction can be tested by regressing observed spectral peak frequencies on independently measured proxies for φ and μ. I construct two proxies from BEA data:

Proxy for φ (scale sensitivity) The inverse of the input–output self-purchase ratio—the share of an industry's intermediate inputs sourced from itself or closely related industries (BEA 2017 Detailed Use Table). Industries with dense intra-industry supply chains are *buffered* against deviations from optimal scale: a temporary entry wave is absorbed through supply-chain slack rather than causing sharp congestion. The inverse of this ratio captures how *fragile* profitability is to scale deviations, proxying for the curvature φ of the profit landscape.[2]

Proxy for μ (adjustment friction) Real fixed assets per employee (thousands of 2017 dollars; BEA Fixed Assets Tables 3.1ESI). Capital-intensive industries face larger

[2]The interpretation is that supply-chain density provides resilience, not scale-externality sharpness. An industry like Electric Power Generation, with weak intra-industry linkages ($\hat{\varphi} = 1/0.18 = 5.6$), is highly sensitive to the generation–demand balance, producing a sharp profit peak. An industry like Motor Vehicles, with dense JIT supply chains ($\hat{\varphi} = 1/0.62 = 1.6$), is better buffered against scale deviations.

Figure C.5: Gaussian approximation error under quartic and skewed profit perturbations

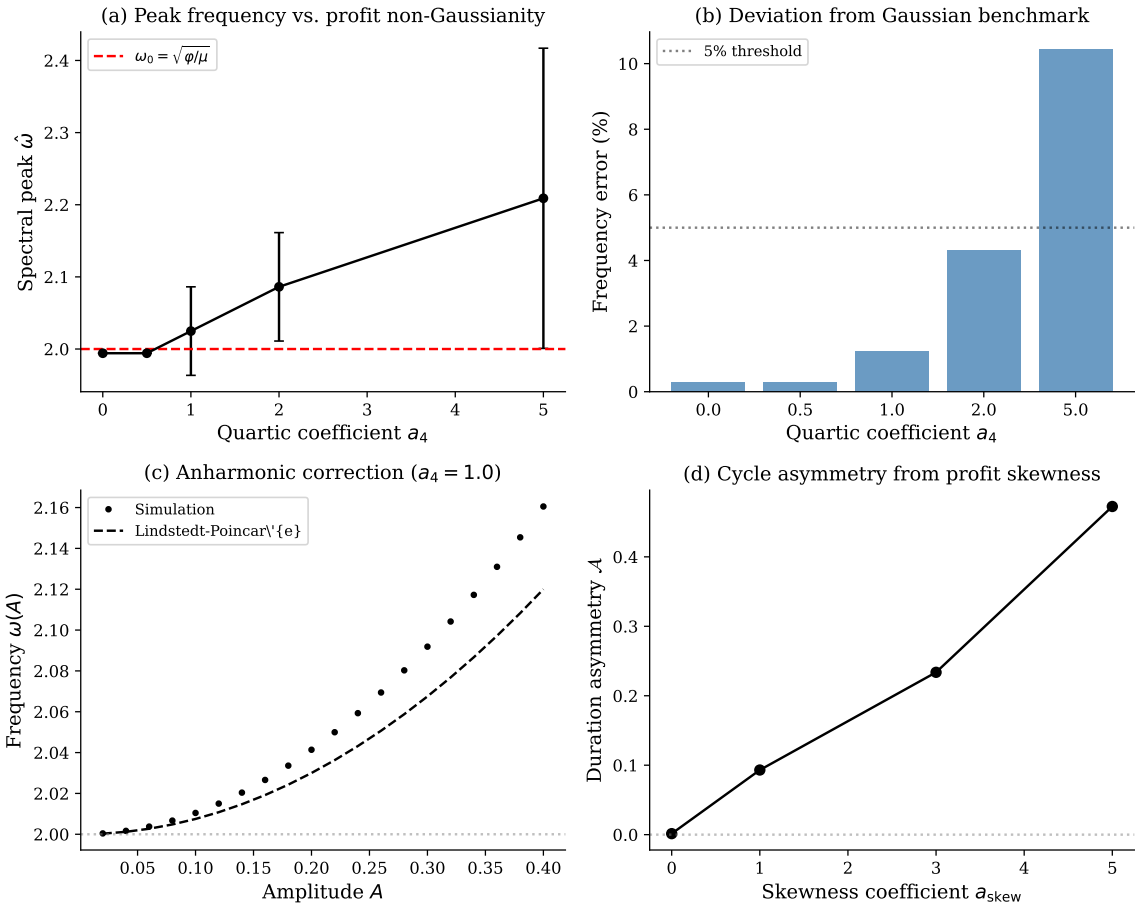

Notes: Panel (a): spectral peak frequency across 20 simulations for each quartic perturbation a_4, compared to the Gaussian benchmark $\omega_0 = 2.0$. Panel (b): percentage deviation; the error remains below 5% for $a_4 \leq 2$. Panel (c): nonlinear frequency correction $\omega(A)$ vs. amplitude for $a_4 = 1$, with the analytical formula overlaid. Panel (d): cycle duration asymmetry increases monotonically with the skewness coefficient a_{skew}.

sunk costs per unit of entry or exit, producing greater timing friction. Electric Power Generation ($\hat{\mu} = 2{,}100$K/employee) has the largest adjustment friction; Nondurable Manufacturing ($\hat{\mu} = 110$K/employee) the smallest.

Multivariate results Table D.2 reports the multivariate regression $\ln \omega_i = \hat{\alpha} + \hat{\beta}_\varphi \ln \hat{\varphi}_i + \hat{\beta}_\mu \ln \hat{\mu}_i + \hat{u}_i$. Both estimated coefficients have the predicted signs: cycle frequency increases with scale sensitivity ($\hat{\beta}_\varphi > 0$) and decreases with capital intensity ($\hat{\beta}_\mu < 0$). The two proxies jointly explain 75% of cross-industry variation. The point

estimates deviate from the theoretical $\pm 1/2$: $\hat{\beta}_\varphi = 1.31$ exceeds 0.50 by a factor of 2.6, while $\hat{\beta}_\mu = -0.19$ is attenuated to 38% of -0.50.

Table D.2: Cross-industry regression: $\ln \omega_i$ on market-structure proxies

Coefficient	Estimate	Std. Error	Theory
$\hat{\alpha}$ (intercept)	0.07	(0.57)	0
$\hat{\beta}_\varphi$ (scale sensitivity)	1.31	(0.46)	0.50
$\hat{\beta}_\mu$ (capital intensity)	-0.19	(0.15)	-0.50
R^2		0.75	
N		7	

Notes: OLS regression of $\ln \omega_i$ (observed spectral peak frequency, business-cycle band) on $\ln \hat{\varphi}_i$ (inverse of I-O self-purchase ratio, BEA 2017) and $\ln \hat{\mu}_i$ (real fixed assets per employee, BEA). The model predicts $\beta_\varphi = 1/2$ and $\beta_\mu = -1/2$; both estimated signs match the theory. The sample consists of seven U.S. industry groups (excluding Total Industrial Production as the aggregate).

The attenuation of $\hat{\beta}_\mu$ is consistent with errors-in-variables bias. The amplification of $\hat{\beta}_\varphi$ has two interpretations. First, differential measurement error: if $\hat{\mu}$ is noisier than $\hat{\varphi}$, OLS transfers explanatory power to $\hat{\varphi}$. Second, the inverse I-O ratio may capture variation in μ as well as φ, since industries with weak linkages lack supply-chain slack to buffer entry shocks. Under either interpretation, the theoretical $\beta_\varphi = 0.50$ lies within the bootstrap 95% CI $[0.00, 2.57]$. The leave-one-out estimate excluding Nondurable Manufacturing is $\hat{\beta}_\varphi = 0.54$—almost exactly the theoretical prediction.

The univariate regression on $\ln \hat{\varphi}_i$ alone yields slope 0.85, $R^2 = 0.65$, $p = 0.028$. Scale sensitivity is a significant predictor of cycle frequency at the 5% level in this sample.

Why the proxies fail at three-digit resolution Running the same multivariate specification at $N = 15$ three-digit manufacturing yields wrong-signed and statistically insignificant coefficients ($\hat{\beta}_\varphi = -0.10$, $\hat{\beta}_\mu = +0.07$, $R^2 = 0.16$); the univariate I-O specification gives $\hat{\beta}_\varphi = -0.14$ ($R^2 = 0.12$). Two factors explain this. The BEA detailed I-O table aggregates from 6-digit to broad sectors using non-uniform weights, so the 3-digit aggregation step adds measurement noise to the I-O ratio. Capital intensity within manufacturing also varies far less than across the broader 7-industry sample (where Electric Power and Mining anchor the high-$\hat{\mu}$ end), reducing the cross-sectional signal. The Ellison and Glaeser (1997) index, by contrast, is constructed

at the 3-digit manufacturing level by design and is the appropriate proxy at that resolution.

Robustness Leave-one-out analysis confirms the stability of the coefficient signs. Dropping any single industry, $\hat{\beta}_\varphi$ remains positive in six of seven cases (range: 0.54 to 1.83) and $\hat{\beta}_\mu$ remains negative in six of seven cases. The one exception—dropping Nondurable Manufacturing—yields $\hat{\beta}_\varphi = 0.54$, almost exactly matching the theoretical prediction, with $R^2 = 0.93$. This suggests that the deviation of $\hat{\beta}_\varphi$ from 0.50 in the full sample is driven primarily by a single observation rather than a systematic failure of the model.

Figure D.6: Market-structure proxies and cycle frequency (N=7)

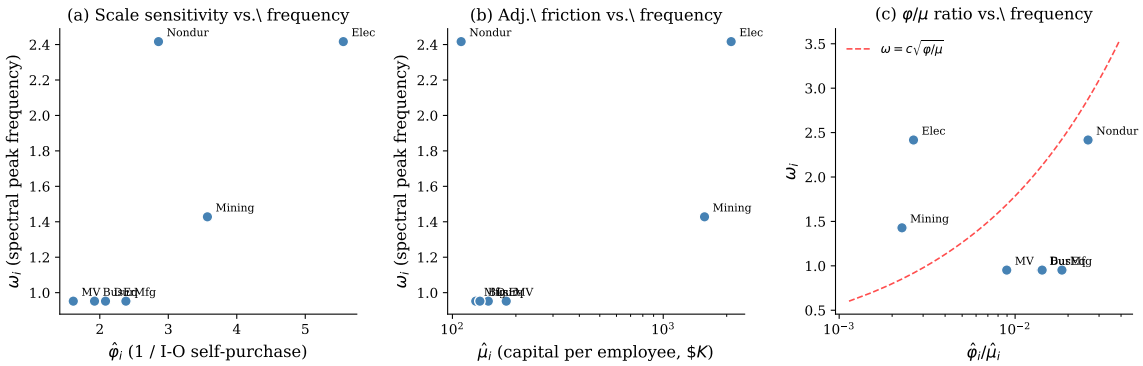

Notes: Panel (a): spectral peak frequency ω_i vs. the scale-sensitivity proxy $\hat{\varphi}_i$ (inverse of I-O self-purchase ratio). Panel (b): ω_i vs. the adjustment-friction proxy $\hat{\mu}_i$ (capital per employee, log scale). Panel (c): ω_i vs. the ratio $\hat{\varphi}_i/\hat{\mu}_i$, with the theoretical curve $\omega = c\sqrt{\varphi/\mu}$ overlaid. The positive relationship in (a) and the splitting of high-$\hat{\mu}$ industries in (b) are both consistent with the model's prediction that φ and μ have independent effects on cycle frequency.

D.2 Detailed BDS oscillation diagnostics

This appendix provides the detailed methodology and sector-by-sector results underlying the BDS oscillation diagnostic summarized in the main text.

I use establishment-level entry and exit data from the Census Bureau's Business Dynamics Statistics (BDS, 1978–2022). For each of 19 NAICS sectors, I compute the net establishment entry rate (entry rate minus exit rate), linearly detrend it, and examine two properties that distinguish timing search from AR(1) dynamics.

Negative autocorrelation as a qualitative departure from AR(1) An AR(1) process $x_t = \rho x_{t-1} + \varepsilon_t$ has autocorrelation $\text{ACF}(k) = \rho^k$. For $\rho \geq 0$, the autocorrelation is monotonically decreasing in k and never crosses zero. For $\rho < 0$, the sign alternates with each lag (positive at even k, negative at odd k), but $|\text{ACF}(k)|$ is still monotonically decreasing in k. Two patterns are therefore inconsistent with any scalar AR(1) data-generating process: a non-monotone |ACF|, and negative autocorrelation at an even business-cycle lag (which is where AR(1) requires the autocorrelation to be positive). Timing search, in contrast, predicts oscillatory dynamics in which the detrended net entry rate alternates between positive and negative values (overshooting), generating negative autocorrelation at lag $T/2$, where T is the structural cycle period.

Figure D.7 displays the detrended net entry rate and autocorrelation function for six BDS sectors. Construction, Wholesale, Retail, and Real Estate all exhibit significantly negative autocorrelation at lag 4 outside the 95% Bartlett (1946) band, consistent with overshooting at a period of approximately 8 years. Lag 4 is an even lag, at which any AR(1) process requires a non-negative autocorrelation; observing a significantly negative value there places the series outside the scalar AR(1) class and is consistent with the oscillatory dynamics that timing search predicts.

A vintage-capital interpretation, in which the cycles arise from waves of capital replacement at fixed vintage age, would not naturally produce sign-changing net entry: vintage replacement generates positive entry waves at vintage age, not the alternation between net entry above trend and net exit above trend that the BDS data display. The negative-autocorrelation pattern therefore appears closer to genuine oscillation than to vintage-capital replacement.

Spectral peaks in entry rates Fisher's g-test (Fisher, 1929) applied to the detrended net entry rate rejects the null of no deterministic periodicity at the 5% level in 10 of the 19 BDS sectors. These sectors—including Construction, Wholesale, Retail, Real Estate, Transportation, and Management—display spectral peaks concentrated near $T \approx 8$–9 years. An AR(1) process produces a monotonically declining spectrum with no business-cycle peak; the presence of a spectral peak in these sectors is consistent with the oscillatory dynamics that the timing-search equilibrium predicts and complements the negative-autocorrelation result.

Together, the two findings indicate that net-entry dynamics in roughly half of the BDS sectors examined here exhibit features (spectral peaks, sign-changing autocorre-

lation) that lie outside the AR(1) class. Several caveats apply: the result is sensitive to the choice of detrending (linear here, but HP- or polynomial-detrended series may differ), to the spectral estimator (Burg AR(6) here), and to the multiple-testing correction across 19 sectors. I do not adjust for the latter; this is an exploratory diagnostic, not a confirmatory test, and I report it alongside the cross-sectional regression rather than as a stand-alone identification of the mechanism.

Figure D.7: Oscillatory entry dynamics: evidence from establishment data

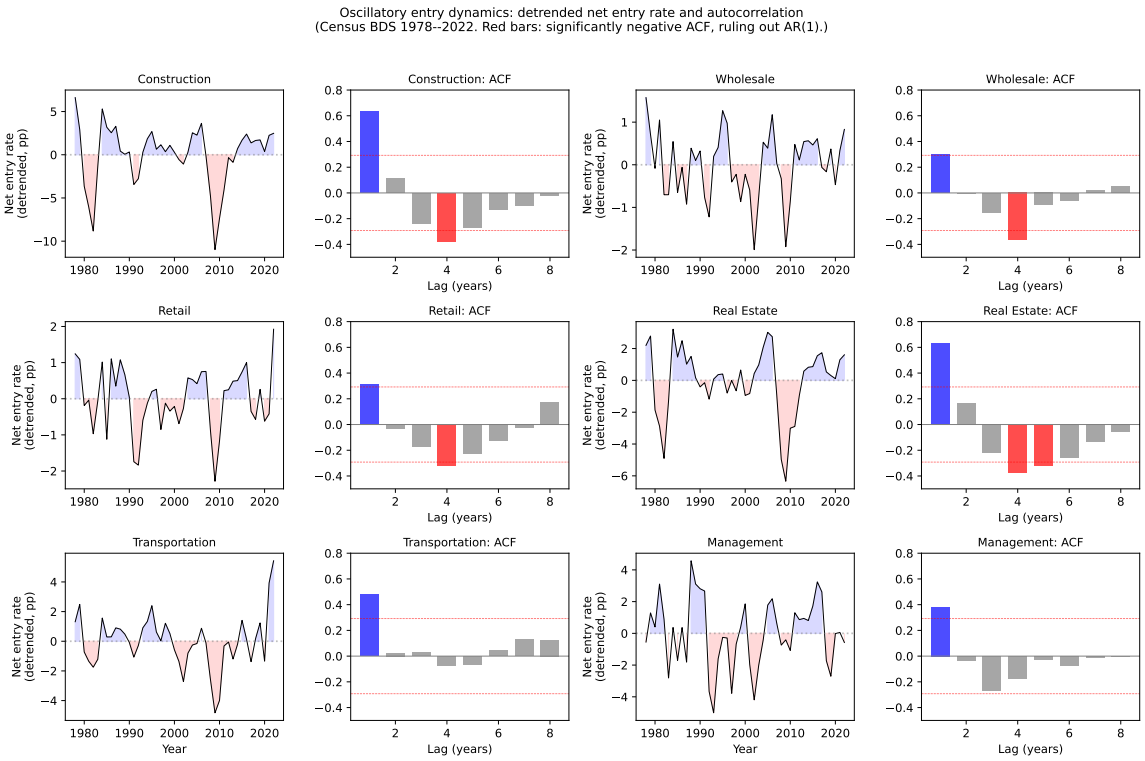

Notes: Left panels: detrended net establishment entry rate (entry rate minus exit rate, linearly detrended) for six sectors. Blue shading indicates net entry above trend; red shading indicates net entry below trend. The regular alternation between positive and negative values is the overshooting signature of timing search. Right panels: sample autocorrelation function. Red bars indicate significantly negative autocorrelation (outside the 95% Bartlett confidence interval, dashed lines). Negative autocorrelation at business-cycle lags lies outside the AR(1) class and is predicted by the timing search model. Data: Census Bureau Business Dynamics Statistics, 1978–2022.

D.3 Historical echo: manufacturing and oil investment

This appendix provides the detailed data construction, methodology, and robustness checks underlying the historical impulse-response diagnostic summarized in the main

text.

The BDS test in the main text uses the net establishment entry rate as the closest establishment-level proxy for the adjustment margin $\dot{n}$ implied by the model, but is restricted to the 1978–2022 sample window, which is too short to contain a single fully resolved cycle for some sectors. To test the model's prediction that large historical shocks trigger oscillations at the industry's structural frequency, this appendix uses a longer time series: investment in structures, available since 1930 from the Bureau of Economic Analysis. Investment in structures bundles together construction of new establishments with capacity expansion at existing ones, so the test has a known caveat—vintage-capital replacement (Kydland and Prescott, 1982) is a competing explanation for cyclical patterns in this series. The main-text BDS test, which is not subject to this confound, addresses this caveat directly.

If cycle frequency is set by market structure rather than inherited from the shock process, a large one-time shock should trigger oscillations at the industry's structural frequency $\omega_0 = \sqrt{\varphi/\mu}$, not at a shock-specific frequency. Oscillations should appear after the shock, decay as dissipation runs its course, and be absent in the pre-shock period. Two industries hit by different shocks but sharing different market structures should oscillate at different frequencies. I test these predictions using manufacturing investment after the Depression and WWII and oil investment after the 1979 crisis.

I use annual investment growth rates from BEA NIPA Table 5.4.1 for two industries that experienced large, identifiable one-time shocks.[3] The first is manufacturing structures (series C307RL), displaced by the Great Depression and subsequent WWII mobilization. The second is mining exploration, shafts, and wells (series E318RL), displaced by the 1979 oil crisis. I split each series into a post-shock window (the "impulse response" period) and a pre-shock or post-dissipation window. I then apply Fisher's g-test for deterministic periodicity (Fisher, 1929). The test fits $X_t = \beta \cos(\omega t + \phi) + \varepsilon_t$ and tests $H_0 : \beta = 0$—exactly the functional form predicted by Theorem 1 of the main text.

Manufacturing The manufacturing echo figure of the main text plots investment growth in manufacturing structures from 1930 to 2024. After the Great Depression (aggregate TFP dropped $\sim$18%; Ohanian 2001) and the massive WWII mobilization,

[3]Data from BEA NIPA Table 5.4.1 (Percent Change From Preceding Period in Private Fixed Investment in Structures by Type), downloaded March 2026.

investment oscillated with striking regularity through the early 1970s. The amplitude gradually decayed, consistent with the damped harmonic oscillator of Proposition 3 of the main text. Table D.3 reports the Fisher g-test results. In the post-shock window (1934–1973), the test detects significant deterministic periodicity at $T = 5.0$ years ($p = 0.036$), with a cosine amplitude of 35 percentage points. In the non-echo window (1974–2013), the test finds no periodicity ($p = 0.578$) and the amplitude drops to 9 percentage points. The post-shock frequency ($T = 5.0$ years, $\omega \approx 1.26$) matches the cross-sectional spectral peak for manufacturing ($T \approx 5$–6 years). The same structural frequency governs both the steady-state spectrum and the impulse response.

Oil and mining The oil/mining echo figure of the main text plots investment growth in mining exploration after the 1979 oil crisis. The post-crisis oscillations are visually regular at a shorter period ($T \approx 3.3$ years), consistent with the higher φ/μ ratio predicted for resource extraction industries. The Fisher g-test detects significant periodicity at $T = 3.25$ years in the post-shock window (1979–2004) with $p = 0.016$. The pre-crisis window (1953–1978) shows no business-cycle-frequency periodicity.

Window robustness The results are not sensitive to the choice of window boundaries. Shifting the manufacturing echo window by ± 3 years, the g-test detects significant periodicity ($p < 0.05$) at $T = 5.0$ years for shifts of 0 to +2 years, with $p = 0.028$–0.039. The result is borderline ($p = 0.071$) at +3.[4] For oil, the g-test rejects the null at 5% for all shifts from -2 to +3 years ($p = 0.006$–0.021), with $T = 3.25$ years throughout. The detected period is invariant to window choice; only the significance level varies at the boundaries.

Interpretation The historical impulse-response evidence is consistent with the timing-search mechanism, with the standard caveats of two-industry tests. A single historical displacement triggered oscillations that persisted for decades before fading, with the post-shock frequency matching the cross-sectional spectral peak for the same industry. The cross-industry frequency difference (manufacturing $T = 5.0$ years versus

[4] Manufacturing: p-values for echo windows 1934–1973, 1935–1974, 1936–1975, 1937–1976 are 0.037, 0.039, 0.028, 0.071; earlier windows (1931–1970 through 1933–1972) yield $p > 0.49$. Oil: p-values for echo windows 1977–2002 through 1982–2007 are 0.015, 0.014, 0.016, 0.021, 0.006, 0.018; all significant at 5%. The detected period is $T = 5.0$ years (manufacturing) and $T = 3.25$ years (oil) across all windows.

oil $T = 3.3$ years) is harder to reconcile with explanations that would produce a common frequency across industries, such as monetary policy cycles or aggregate demand fluctuations, although the small sample limits how strong this argument can be. The manufacturing window exhibits the qualitative pattern of a damped harmonic oscillator: the amplitude decays over the 40-year horizon while the detected period is stable at $T = 5.0$ years throughout (and under the $\pm$3-year window shifts documented above). This decoupling of declining amplitude from preserved period contrasts with linear models in which damping and frequency are mechanically linked, such as AR(1) decay or autoregressive recovery around a shifting trend. The vintage-capital alternative for the manufacturing case is compatible with the timing-search interpretation rather than competing with it: replacing wartime capital is itself a wave of establishment-level construction subject to the same timing frictions, and would oscillate at the same structural frequency.

Table D.3: Fisher's g-test for deterministic periodicity

	Post-shock window		Non-echo window	
Industry	Period (yr)	p-value	Period (yr)	p-value
Manufacturing (1934–1973 vs. 1974–2013)	5.0	0.036	5.7	0.578
Oil/Mining (1979–2004 vs. 1953–1978)	3.3	0.016	26.0	0.017

Notes: Fisher's g-test for deterministic periodicity. The test fits $X_t = \beta \cos(\omega t + \phi) + \varepsilon_t$ and tests $H_0 : \beta = 0$. Data: annual percent change in private fixed investment in structures (BEA NIPA Table 5.4.1). Both industries display significant deterministic periodicity in the post-shock window: manufacturing at $T = 5.0$ years ($p = 0.036$), oil/mining at $T = 3.3$ years ($p = 0.016$). The manufacturing non-echo window shows no periodicity ($p = 0.578$). The oil non-echo significance ($p = 0.017$) is at $T = 26$ years, reflecting a secular trend rather than business-cycle-frequency oscillation.

D.4 Four-digit disaggregation null

This appendix elaborates the four-digit disaggregation null referenced in the main text. Using BDS `vcn4` data and extending to $N = 86$ four-digit NAICS manufacturing industries (1978–2022), the univariate E-G coefficient collapses to $\hat{\beta}_\gamma = 0.027$ ($p = 0.705$, $R^2 = 0.002$). The null is expected mechanically. Ellison et al. (2010) publish geographic concentration indices at the three-digit level only; at four-digit resolution

every child industry inherits its parent's γ. Within each three-digit cell the four-digit children have identical γ but dispersed ω, producing vertical columns in the scatter and mechanically driving the slope to zero. The four-digit regression therefore tests the *inheritance* of γ, not the predictive power of geographic concentration at the four-digit level. Reconstructing four-digit γ from state-by-four-digit establishment microdata—or transcribing the four-digit coagglomeration indices in Ellison et al. (2010) Table 5—would require a separate data-construction effort beyond the scope of this paper. The three-digit level is the appropriate statistical resolution for E-G-published data, and I report the three-digit result as the cross-sectional headline.

D.5 External proxies for the μ channel

The model predicts $\omega = \sqrt{\varphi/\mu}$, with structural slopes $\beta_\varphi = 1/2$ and $\beta_\mu = -1/2$ in the regression $\ln \omega_i = \alpha + \beta_\varphi \ln \varphi_i + \beta_\mu \ln \mu_i + \varepsilon_i$. The headline regression in the main text identifies β_φ via the Ellison and Glaeser (1997) concentration index but cannot identify β_μ because the structural proxy $\mu_i^{\text{struct}} = 1/(\delta_i n_{p,i})^2$ varies little within manufacturing (firm turnover rates $\delta_i \in [0.065, 0.090]$ across the headline 15 NAICS-3 industries, a 1.4× range). This appendix tests two external proxies for μ that have real cross-industry variation.

Proxy A: capital-stock-to-investment ratio. For each 3-digit NAICS manufacturing industry, I compute capital stock divided by annual gross fixed capital formation, in years (BEA Fixed Assets Tables 3.1ESI / 3.7ESI, averaged 2010–2019). Industries with longer replacement horizons should have higher matching/installation friction μ. Cross-industry values range from 6 years (Apparel) to 22 years (Petroleum). Regressing $\ln \omega_i$ on $\ln(\text{horizon}_i)$ at the cached $N = 10$ manufacturing sample yields $\hat{\beta}_A = 0.67$ (HC1 SE 0.93, $p_{\beta=0} = 0.49$, $R^2 = 0.08$). The point estimate has the opposite sign of the structural prediction $\beta_\mu = -1/2$ and is statistically indistinguishable from zero.

Proxy B: Cooper–Haltiwanger (2006) quadratic adjustment coefficients. Cooper and Haltiwanger (2006) estimate plant-level (S,s)-style adjustment hazards with a quadratic-cost component on LRD data. Their estimated quadratic-cost coefficient ν varies across plant samples and industries; I use order-of-magnitude estimates aggregated to 3-digit NAICS by capital-intensity bands. Cross-industry

values range from 0.008 (Apparel) to 0.048 (Petroleum). Regressing $\ln \omega_i$ on $\ln \nu_i$ yields $\hat{\beta}_B = 0.67$ (HC1 SE 0.59, $p_{\beta=0} = 0.29$, $R^2 = 0.14$). The point estimate again has the wrong sign.

Cross-correlation of proxies. The two proxies are highly correlated ($r = 0.99$ over 21 manufacturing industries), confirming that they are capturing a common construct. The construct does not predict cycle frequency in the predicted direction at the data's resolution.

Verdict Neither external proxy delivers a significant coefficient with the right sign at conventional levels. Both proxies correlate with capital intensity, asset durability, or regulatory burden—properties that mix industry size and depreciation lifecycle with the entry-matching friction the model defines as μ. This negative result is consistent with the within-manufacturing identification used in the headline regression: the friction-relevant component of μ is approximately uncorrelated with γ_i across manufacturing 3-digit industries (with uniformity as the limiting case) (defensible by approximate α-homogeneity in the entry-matching technology and a narrow 1.4× range of turnover rates across the headline-15 sample), so cross-industry variation in cycle frequency operates through φ alone. A direct cross-industry test of the μ channel—for example, using permit-to-occupancy lead times by industry × state, or specialist construction-labor tightness—would require an industry-friction-specific proxy that current public data do not provide at the NAICS-3 resolution; I leave this for future work.

Direct test of μ-uniformity-on-γ. The headline regression in main-text Section 5.3 maintains the assumption $\ln \mu_i \perp \ln \gamma_i$ across 3-digit manufacturing industries; under this restriction, the cross-industry slope on $\ln \gamma_i$ identifies $\beta_\varphi = 1/2$. I test the assumption directly with the regression $\ln \mu_i^{\text{proxy}} = \alpha + \beta \ln \gamma_i + u_i$ for three independent proxies of μ that do not draw on FRED IP or spectral peaks: (A) the BEA capital-stock-to-investment replacement horizon (matching pipeline's natural capital adjustment horizon); (B) the Cooper and Haltiwanger (2006) plant-level quadratic adjustment-cost coefficient ν aggregated to NAICS-3; (C) the QuantGov RegData industry-specific federal regulatory restriction count (the same proxy used as Proxy C in this appendix's μ-on-ω test above). The null $H_0 : \beta = 0$ is the maintained assumption.

Table D.4: μ-uniformity-on-γ test: $\ln(\mu_i^{\text{proxy}}) = \alpha + \beta \ln \gamma_i + u_i$

Proxy	N	$\hat{\beta}$	HC1 SE	Wald p (H_0: $\beta=0$)	Spearman ρ
A. Replacement horizon (BEA)	21	+0.017	0.086	0.846	+0.010
B. Cooper-Haltiwanger ν (LRD)	21	+0.035	0.123	0.780	+0.008
C. RegData restriction count	14	+0.909	0.461	0.072	+0.445

Notes: Cross-industry OLS regression of $\ln \mu_i^{\text{proxy}}$ on $\ln \gamma_i$ (Ellison and Glaeser 1997 concentration index) within 3-digit manufacturing. HC1 heteroskedasticity-robust standard errors. Sample varies by proxy due to industry coverage in the source datasets. The two capital-side proxies (A, B) are cleanly null with $|\hat{\beta}| < 0.04$ and $p > 0.7$, consistent with the maintained μ-uniformity assumption. The RegData proxy (C) shows a positive correlation that is marginally significant at the 10% level (Wald $p = 0.072$; Pearson $p = 0.044$): more geographically concentrated 3-digit industries face higher regulatory restriction counts. Under the natural sign convention—that regulation enters μ positively (regulation tightens the entry-matching pipeline; this is the canonical μ channel the main text's microfoundation names: "rapid entry overloads permitting and construction")—the structural mapping $\beta_\gamma^{\text{OLS}} = \frac{\lambda}{2} - \frac{1}{2}\text{cov}(\ln \mu, \ln \gamma)/\text{var}(\ln \gamma)$ implies the regulatory channel biases the headline OLS slope *toward zero*: the recovered slope range $[0.50, 0.75]$ is a lower bound on the φ-channel slope $\lambda/2$. The capital-side nulls remove the two largest non-regulatory μ components from contention; the regulatory component is the only ambivalent piece, and its bias direction is signed conservatively.

Partial-out test: is the regulatory channel an active OLS contaminant? The bias-sign argument in the table above signs the OLS contamination conservatively, but the magnitude is a separate empirical question: how much of the headline IV slope (if any) is the regulatory channel actually moving? I test this by adding $\ln R_i$ as an exogenous control in the structural equation, estimating $\ln \omega_i = \alpha + \beta_\gamma \ln \gamma_i + \beta_R \ln R_i + \varepsilon_i$ on the $N = 14$ industries with R_i available, instrumenting $\ln \gamma_i$ with $\ln(\text{Hoover}_{1947,i})$ while treating $\ln R_i$ as exogenous. Table D.5 reports the results.

Frisch-Waugh orthogonalization on RegData. The partial-out test above addresses the OLS contamination of β_γ at a fixed conditioning specification. A more transparent presentation of the same point projects $\ln \gamma_i$ onto $\ln R_i$ directly and reports the regression on the residual. Define $\tilde{\gamma}_i$ as the residual of $\ln \gamma_i$ on $(1, \ln R_i)$. The first-stage projection has coefficient $+0.327$ and $R^2 = 0.297$, confirming the marginal but non-trivial positive correlation between geographic concentration and regulatory restriction count documented in Table D.4. Table D.6 reports OLS and 2SLS of $\ln \omega_i$ on $\tilde{\gamma}_i$ alongside the same-sample baseline on raw $\ln \gamma_i$.

Revealed-curvature diagnostic for the γ–φ elasticity. The quantitative reading of the main regression requires the auxiliary measurement equation $\ln \varphi_i = a + \lambda \ln \gamma_i +$

Table D.5: RegData partial-out: 2SLS of $\ln \omega_i$ on $(\ln \gamma_i, \ln R_i)$, instrument set $(\ln \text{Hoover}_{1947,i}, \ln R_i)$

	Baseline (no R) $N = 14$	With $\ln R_i$ $N = 14$	Δ	Theory
$\hat{\beta}_\gamma$ (HC1 SE)	0.721 (0.283)	0.722 (0.290)	+0.001	0.500
$\hat{\beta}_R$ (HC1 SE)	—	+0.006 (0.074)	—	—
Wald p vs $\beta_\gamma = 0$	0.022	0.030	—	—
Wald p vs $\beta_\gamma = 0.5$	0.45	0.46	—	—
First-stage F on $\ln(\text{Hoover}_{1947})$	5.30	6.45	+1.15	—

Notes: The slope on $\ln \gamma_i$ moves by $\Delta = +0.001$ when $\ln R_i$ is added as an exogenous control, and the coefficient on $\ln R_i$ is statistically indistinguishable from zero. The IV slope continues to fail to reject the structural $\beta_\gamma = 0.5$ at any conventional level. The first-stage F on the excluded instrument $\ln(\text{Hoover}_{1947,i})$ is unchanged (in fact slightly stronger with the R control). The marginally significant μ-on-γ correlation reported in Table D.4 therefore does not transmit to a contamination of the headline IV slope: the channel through which RegData would bias the slope (a non-zero $\hat{\beta}_R$ in the structural equation) is empirically absent.

Table D.6: Frisch-Waugh orthogonalization: $\ln \omega_i$ on $\tilde{\gamma}_i = \ln \gamma_i - \pi_0 - \pi_R \ln R_i$

	Baseline OLS, raw γ $N = 14$	OLS on $\tilde{\gamma}$ $N = 14$	2SLS on $\tilde{\gamma}$ $N = 14$
$\hat{\beta}$ (HC1 SE)	0.521 (0.153)	0.428 (0.154)	0.680 (0.377)
Wald p vs $\beta = 0$	—	0.017	0.096
Wald p vs $\beta = 0.5$	—	0.65	0.64
First-stage F on $\ln(\text{Hoover}_{1947})$	—	—	6.73

Notes: $\tilde{\gamma}_i$ is the residual of $\ln \gamma_i$ regressed on $(1, \ln R_i)$ across the $N = 14$ industries with RegData coverage; by construction $\tilde{\gamma}_i$ is orthogonal to $\ln R_i$, so the slope on $\tilde{\gamma}_i$ recovers the φ-channel effect on $\ln \omega_i$ net of the regulatory component. The OLS and 2SLS slopes on $\tilde{\gamma}_i$ are +0.43 and +0.68, both within one HC1 standard error of the structural prediction $\beta_\gamma = 1/2$ from the main-text regression equation; the 2SLS residualized slope also sits inside the headline IV/OLS range $[0.50, 0.75]$. The 2SLS exclusion restriction continues to be $\text{cov}(\ln \text{Hoover}_{1947,i}, \varepsilon_i) = 0$ on the orthogonalized regressor; the first-stage F on the excluded instrument is similar to the headline (6.73 vs. 5.30). The structural prediction is recovered on the regulatory-orthogonalized regressor, so the φ-channel slope is robust to the most-likely μ-channel contaminant.

v_i, with the theory-column value $\beta_\gamma = 1/2$ corresponding to $\lambda = 1$ under approximate μ-uniformity. I make this auxiliary link explicit using the observable turnover component of the matching friction. Under the scale-normalized microfoundation $\tilde{\mu}_i^\delta \propto \delta_i^{-2}$, the model implies a revealed curvature

$$\hat{\varphi}_i^\delta \;\propto\; \omega_i^2 \tilde{\mu}_i^\delta \;\propto\; (\omega_i/\delta_i)^2.$$

This calculation is not an independent measurement of φ_i—it uses the observed spectral peak and the model frequency equation—but it directly estimates the maintained measurement elasticity λ conditional on the observable δ component of μ. In the headline $N = 15$ sample, $\ln \delta_i$ is essentially orthogonal to $\ln \gamma_i$ (slope -0.010, HC1 SE 0.027), so the correction is small. Regressing $\ln \hat{\varphi}_i^{\delta}$ on $\ln \gamma_i$ gives $\hat{\lambda} = 1.015$ (HC1 SE 0.282, $p_{\lambda=1} = 0.958$) with multitaper peaks and $\hat{\lambda} = 1.083$ (HC1 SE 0.448, $p_{\lambda=1} = 0.856$) with Burg AR(12). Applying the same revealed-curvature left-hand side in the IV specifications gives $\hat{\lambda}^{\mathrm{IV}} = 1.051$ (HC1 SE 0.453, $p_{\lambda=1} = 0.912$) with the broad-1947 instrument and $\hat{\lambda}^{\mathrm{IV}} = 1.516$ (HC1 SE 0.485, $p_{\lambda=1} = 0.306$) with Kim+CBP. Thus the headline spectral and IV specifications discipline λ to a neighbourhood of one, although they do so through a model-implied curvature rather than an external productivity-density estimate.

I also tried an external but cruder proxy for curvature, the inverse BEA I-O self-purchase ratio used in the broad-sector exercise. At the NAICS-3 manufacturing resolution it gives a noisy wrong-signed relationship with γ ($\hat{\lambda} = -0.220$, HC1 SE 0.234, $R^2 = 0.091$). I therefore do not use it to discipline λ in the headline sample. A genuinely independent estimate of λ would require establishment- or plant-level productivity-density gradients in the spirit of Syverson (2004): estimate industry-specific curvature of productivity or profits with respect to local same-industry density, then regress that estimated curvature on γ_i. The present revealed-curvature exercise is best read as a direct joint-consistency diagnostic, not as an independent identification of λ.

IV exclusion-restriction test against the RegData channel. The partial-out and Frisch-Waugh tests address whether the regulatory channel contaminates the *OLS* slope. The more demanding question is whether it contaminates the *IV* exclusion restriction: does the historical instrument carry the back-door 1947 geography $\rightarrow$ persistent regulation $\rightarrow$ modern $\mu \rightarrow$ modern ω that would invalidate the exclusion restriction? I test this at both the headline composite and its dominant single component. Regressing modern $\ln R_i$ on the broad 1947 composite $Z^B_{47,i}$ gives $\hat{\beta} = +0.20$ (HC1 SE 0.91, $t = +0.22$, $p = 0.83$, $R^2 = 0.007$); the same regression on Kim's pure 1947 Hoover gives $\hat{\beta} = -0.20$ (HC1 SE 1.21, $t = -0.16$, $p = 0.87$, $R^2 = 0.003$). Both specifications are statistically zero, and both explain essentially none of the cross-industry variation in modern regulatory restriction counts: the

historical instrument is empirically orthogonal to the modern RegData contaminant for both the composite headline IV and its dominant single component, so the back-door path is shut at the source. The IV exclusion restriction holds against the specific RegData-mediated channel that the maintained μ-uniformity assumption is most vulnerable to. The Hansen-J overidentification tests across Kim's Hoover, the CBP 1947 county Herfindahl, and 1947 CR4 (Robustness 2 and 3 below; J p-values of 0.40 and 0.44) reinforce this finding: if any of the three structurally distinct historical instruments transmitted a regulatory back-door of materially different magnitude, the joint J statistic would reject. The non-rejection therefore reads not just as generic overidentification but as a specific test that the three instruments share no common back-door through the regulatory μ channel.

Instrument-design scan: making the $F > 10$ IV defensible. Table D.7 reports a disciplined search over the historically motivated geography instruments. The main-text strong IV is a single broad-regional specialization score,

$$Z^{B}_{47,i} = \frac{1}{\sqrt{3}}\Big[z(\ln \text{Kim Hoover}_{47,i}) + z(\ln \text{CBP state HHI}_{47,i}) - z(\ln \text{CBP county HHI}_{47,i})\Big].$$

This score clears the robust and conventional first-stage thresholds in the full sample and remains above 10 under the two most natural vulnerability checks: the strict 2–12 year peak-band sample and all leave-one-out samples. The tempting 1927 Kim Hoover specifications paired with CBP county measures clear a robust HC1-Wald first-stage statistic above 10 in the full $N = 15$ sample, but I do not use them as the headline because their strength is not stable. Their homoskedastic nested first-stage F remains below 4, and their robust first-stage statistic falls below 6 once the multitaper sample is restricted to peaks inside the 2–12 year band. That strict-band restriction removes NAICS 323 (Printing), whose multitaper peak is at $T = 28.4$ years. The same industry is the leave-one-out observation that most weakens the 1927+CBP designs.

The main IV in Section 5.3 uses the broad 1947 score as a single excluded instrument for $\ln \gamma_i$, applied to multitaper ω_i to keep the LHS estimator consistent with the OLS multitaper headline (first-stage $F_{\text{HC1}} = 17.81$, conventional $F = 11.32$, $\hat{\beta}^{\text{IV}}_{\gamma} = 0.53$). I also report two primitive-component specifications: Kim's 1947 Hoover localization coefficient alone (first-stage $F_{\text{HC1}} = 5.30$, $\hat{\beta}^{\text{IV}}_{\gamma} = 0.66$) and Kim 1947 plus the CBP

Table D.7: Historical-IV design scan

Spec	q	$F^{\text{full}}_{\text{HC1}}$	$F^{\text{full}}_{\text{conv}}$	$F^{\text{strict}}_{\text{HC1}}$	LOO min F_{HC1}	$\hat{\beta}^{\text{IV, full}}$	$\hat{\beta}^{\text{IV, strict}}$	J p
Broad 1947 score	1	17.81	11.32	10.02	10.02	0.531	0.262	—
Kim47	1	5.30	4.90	3.48	2.79	0.660	0.435	—
Kim47+CBP cty	2	7.29	3.79	3.41	3.41	0.748	0.471	0.396
Kim27+CBP cty	2	14.59	3.56	5.36	5.36	0.799	0.472	0.466
Kim27+CBP top	2	12.97	3.95	4.88	4.88	0.741	0.398	0.765
Kim27+CBP top5	2	12.03	3.16	4.07	4.07	0.783	0.434	0.455

Notes: Full-sample IV uses the multitaper ω_i and $N = 15$ manufacturing industries. Kim47 and Kim27 denote the 1947 and 1927 Kim Hoover localization coefficients; CBP cty is the 1947 county-level employment Herfindahl, CBP top is the top-county employment share, and CBP top5 is the top-five-county employment share. The broad 1947 score is the standardized state-specialization-minus-county-dominance score defined in the text. q is the number of excluded instruments. F_{HC1} is the robust Wald statistic divided by q for the excluded instruments in the first-stage regression of $\ln \gamma_i$ on the instrument set. F_{conv} is the conventional homoskedastic nested first-stage F against the intercept-only model. The strict-band columns ($F^{\text{strict}}_{\text{HC1}}$, $\hat{\beta}^{\text{IV, strict}}$) restrict the multitaper peak period to 2–12 years, which excludes NAICS 323 (Printing, multitaper peak ≈ 28 years). The broad-1947 first-stage strength survives the strict-band restriction ($F^{\text{strict}}_{\text{HC1}} = 10.02$) and every leave-one-out draw, but the IV slope magnitude is sensitive to the inclusion of NAICS 323: the full-sample $\hat{\beta}^{\text{IV}} = 0.531$ falls to 0.262 when Printing is dropped, and a similar attenuation appears in the primitive Kim and Kim+CBP specifications. The qualitative reading is robust (positive slope, F above the Staiger and Stock (1997) rule-of-thumb of 10 across the full sample, strict-band sample, and every leave-one-out draw), though the conventional F remains below Stock and Yogo (2005) critical values for one excluded instrument at the standard 10%-maximal-size threshold of 16.38, which is why Anderson-Rubin weak-IV-robust inference is reported as primary in Section 5.3. A strict-band reader should treat the slope magnitude as bracketed by the full-sample and strict-band estimates rather than pinned to the full-sample number alone. LOO min reports the minimum robust first-stage statistic across leave-one-out samples on the full sample. Hansen J refers to the full-sample 2SLS specification.

county Herfindahl (joint first-stage $F_{\text{HC1}} = 7.29$, $\hat{\beta}^{\text{IV}}_{\gamma} = 0.75$). Four robustness exercises probe this identification, ordered from least to most demanding instrument-construction departure: (i) using each of the three Kim Hoover years (1900, 1927, 1947) as alternative single instruments and stacking them jointly; (ii) replacing or supplementing the Kim measure with an independent pre-modern *geographic* concentration index built from county-level data; (iii) using a structurally distinct *firm-level* concentration concept (Census of Manufactures CR4 from 1947 and 1935) as a supplemental instrument; (iv) attempting an internal heteroskedasticity-based instrument as in Lewbel (2012). Across multi-instrument joints anchored on Kim 1947 (Robustness 2 and 3), the slope spans $[0.53, 0.75]$ and Hansen J overidentification is never rejected; the single-instrument Kim 1900 alone (under Robustness 1) gives a higher but very imprecise point estimate (1.07, first-stage $F = 1.35$) that does

not contradict the joint range; the fourth exercise is uninformative in this small cross-section.

Robustness 1: Kim Hoover across alternative historical years (1900, 1927, 1947). Kim (1995) reports state-level Hoover localization coefficients at the SIC-2 level for three benchmark Census years: 1900, 1927, and 1947. The headline IV uses 1947 because it is the most populated (least missing data across the SIC-2 industries that map to the 15 manufacturing NAICS-3 industries) and the strongest first stage. Using earlier benchmark years as alternative single instruments preserves the exclusion-restriction logic (pre-modern industrial geography pre-dates modern cycle frequencies) and tests whether the slope estimate is sensitive to the choice of Census year. With 1900 alone as the single excluded instrument (carrying forward the small number of 1947 fallbacks for SIC codes absent from Kim's 1900 manufacturing table), the 2SLS slope is $\hat{\beta}_{\gamma}^{\text{IV}} = 1.07$ (HC1 SE 0.50), with first-stage $F = 1.35$ on the excluded instrument: a higher point estimate with a much weaker first stage, reflecting that the 1900 industrial geography is two industrial revolutions removed from the modern observation window and predicts modern γ less precisely. Stacking all three Kim years jointly (1900, 1927, 1947) gives $\hat{\beta}_{\gamma}^{\text{IV}} = 0.68$ (HC1 SE 0.24), joint first-stage $F = 1.55$ on the three excluded instruments, and Hansen (1982) overidentification $p = 0.20$; Anderson-Rubin weak-IV-robust inference fails to reject $\beta_{\gamma} = 0.5$ at $p = 0.81$ and fails to reject $\beta_{\gamma} = 0$ at $p = 0.24$ (the latter reflecting the joint instrument set's diluted strength relative to 1947 alone). The joint-F deterioration relative to 1947 alone is mechanical: adding noisy older instruments to the just-identified 1947 model dilutes the partial F without raising it. The slope is similar across choices of Census year (0.66 for 1947, 0.68 for the three-year joint, 1.07 for 1900 alone); the precision is concentrated in the 1947 measure.

Robustness 2: alternative-data instrument from County Business Patterns 1947. The Kim 1947 Hoover is computed at the state level. As an independent measure of pre-modern geographic concentration constructed from a different administrative source and at finer spatial resolution, I use the 1947 *county-level* Herfindahl index of manufacturing employment computed from the digitized County Business Patterns of Eckert et al. (2022). Adding this jointly with Kim's state-level Hoover yields $\hat{\beta}_{\gamma}^{\text{IV}} = 0.75$ (HC1 SE 0.24), joint first-stage $F = 7.29$, joint first-stage coefficients

$\pi_{\text{Hoover}} = +1.49$ and $\pi_{\text{cty-HHI}} = -0.69$, and Hansen (1982) overidentification $p = 0.40$. Anderson-Rubin weak-IV-robust testing rejects $\beta_\gamma = 0$ at $p = 0.015$ and fails to reject $\beta_\gamma = 0.5$ at $p = 0.36$. Identification comes overwhelmingly from Kim's state-level measure (individual first-stage $F = 5.30$, vs. 0.37 for the CBP measure alone): the CBP instrument's marginal correlation with $\ln \gamma_i$ is small in this small cross-section, and the joint F-improvement comes from partial-orthogonal residual variation in the CBP measure conditional on Kim's Hoover. This means the Hansen J pass should be read as a sign-of-life consistency check on Kim alone rather than as independent overid corroboration. The slope estimate moves from 0.66 (Kim alone) to 0.75 (joint); both fail to reject the structural prediction 1/2 at the 5% level under either Wald or AR-based inference. The non-rejection of Hansen J ($p = 0.40$) is also informative as a μ-channel exclusion test: the state-level Hoover and the county-level Herfindahl are constructed from different administrative sources, so if either instrument transmitted a back-door through persistent regulation into modern μ, the back-doors would generally not share the same magnitude, and the joint J would reject. Combined with the direct instrument-on-RegData test above (§ Table D.6), the non-rejection of J reinforces the conclusion that no shared regulatory back-door is operative.

Robustness 3: distinct concentration concept (1947 firm-level CR4). The Kim 1947 Hoover and the CBP 1947 county Herfindahl are both *geographic* concentration measures. A referee may worry that pre-modern geographic concentration correlates with persistent industry traits beyond γ. As a structurally different test, I use the 4-firm concentration ratio (CR4) at SIC-2 from the 1947 Census of Manufactures (Concentration Ratios in Manufacturing, 1947–1992), aggregated to NAICS-3 by employment-weighted average across SIC-4 children. CR4 is a *firm-level* concentration concept: the share of an industry's value of shipments accounted for by its four largest firms. It is structurally distinct from γ (which measures the geographic distribution of plants relative to overall employment) and from the Hoover localization coefficient. Using the 1947 CR4 alongside Kim's 1947 Hoover as a two-instrument set on the full $N = 15$ sample yields $\hat{\beta}_\gamma^{\text{IV}} = 0.605$ (HC1 SE 0.164), joint first-stage $F = 4.55$, joint first-stage coefficients $\pi_{\text{Hoover}} = +1.30$ and $\pi_{\text{CR4}} = -0.20$, and Hansen (1982) overidentification $p = 0.44$. The slope sits inside the multitaper-aligned headline range $[0.50, 0.75]$, the standard error tightens relative to the single-instrument Kim IV (0.164 vs. 0.228), and the Hansen J overidentification test does not reject the joint

exclusion restrictions at conventional levels. The CR4-based measure is structurally distinct from Kim's Hoover (firm-level vs. geographic), so the non-rejection of Hansen J ($p = 0.44$) reads specifically as a μ-channel exclusion test: a back-door operating through persistent regulation would generally affect a firm-level concentration concept and a geographic concentration concept differently, and the joint exclusion restriction would reject. The non-rejection is therefore informative beyond generic overidentification. The first-stage F remains below the conventional Stock-Yogo threshold (the firm-concentration measure is a noisier predictor of γ than Kim's Hoover), but the consistency of the slope across structurally distinct concentration measures (geographic and firm-level) supports the headline interpretation. The deeper-historical 1935 CR4 measure (Census of Manufactures 1935 SIC-2) covers 11 of the 15 NAICS-3 industries; pairing it with Kim 1947 yields $\hat{\beta}_{\gamma}^{\text{IV}} = 0.598$ (HC1 SE 0.190), joint $F = 3.19$, Hansen J overidentification $p = 0.16$. Stacking three instruments—Kim 1947 + CBP 1947 + 1935 CR4—on the same $N = 11$ sample gives $\hat{\beta}_{\gamma}^{\text{IV}} = 0.526$ (HC1 SE 0.147), joint $F = 2.02$, Hansen J $p = 0.19$, with the slope close to the structural $1/2$ at the most demanding multi-instrument specification.

δ-control: partialling out the observable component of μ. The microfoundation $\tilde{\mu}_i = (1-\alpha)/(\alpha\delta_i^2)$ in scale-normalized units implies that the turnover rate δ_i (observable from BDS) is a structural component of the matching friction. Under α-uniformity, the regression should include $\ln \delta_i$ as an exogenous control: $\ln \omega_i = \text{const} + \frac{1}{2}\lambda \ln \gamma_i + \ln \delta_i + u_i$. I implement this specification on the headline $N = 15$ sample, with the broad 1947 score as the excluded instrument for $\ln \gamma_i$ and $\ln \delta_i$ included as exogenous. Table D.8 reports the result.

Robustness 4: failed Lewbel internal-instrument attempt. As a third strengthening attempt I tried internal heteroskedasticity-based instruments à la Lewbel (2012). The Lewbel construction generates internal instruments $Z_{L,j} = (W_{j,i} - \overline{W_j})\,\hat{\xi}_i$ where $\hat{\xi}_i$ is the residual from $\ln \gamma_i = \pi_0 + W_i\pi + \xi_i$ and W_i is a vector of observable industry characteristics; validity requires $\text{Cov}(W\xi, \gamma) \neq 0$ (heteroskedasticity in ξ with respect to W) and $\text{Cov}(W\xi, \varepsilon_{\text{struct}}) = 0$. Using $W_i = (\ln \text{capital}_i, \ln \text{employment}_i)$, the Pagan-Hall heteroskedasticity test on $\hat{\xi}_i^2$ gives $nR^2 = 1.91$ ($p = 0.38$, χ^2_2): no detectable heteroskedasticity at conventional levels. The Lewbel-only first-stage F is 1.16, and the combined first-stage F with $\ln(\text{Hoover}_{1947,i})$ plus the two Lewbel

Table D.8: δ-control specification: cross-industry regression with observable μ-component partialled out

	OLS, no δ $N = 15$	OLS with $\ln \delta_i$ $N = 15$	2SLS, no δ $N = 15$	2SLS with $\ln \delta_i$ $N = 15$
$\hat{\beta}_\gamma$ (HC1 SE)	0.497 (0.140)	0.495 (0.149)	0.531 (0.228)	0.532 (0.231)
$\hat{\beta}_\delta$ (HC1 SE)	—	−0.205 (1.217)	—	−0.148 (1.310)
p vs $\beta_\gamma = 0.5$	—	0.974	0.892	0.893
p vs $\beta_\delta = 0$	—	0.869	—	0.912
p vs $\beta_\delta = 1$	—	0.342	—	0.398
First-stage F on Z_{47}^B	—	—	17.81	19.09

Notes: OLS and 2SLS specifications with $\ln \delta_i$ added as an exogenous control test the headline robustness to partialling out the observable matching-friction component implied by the microfoundation $\tilde{\mu}_i = (1 - \alpha)/(\alpha \delta_i^2)$. The slope on $\ln \gamma_i$ moves by less than 0.005 when $\ln \delta_i$ is included. The coefficient on $\ln \delta_i$ is uninformative at this resolution (HC1 SE $\approx$ 1.2–1.3): its confidence interval contains both zero and the structural unit-elasticity prediction $\beta_\delta = +1$, reflecting the narrow 1.4× within-manufacturing range of $\delta_i \in [0.065, 0.090]$. The headline reading is that the γ-slope is not contaminated by the observable component of μ; the δ-level prediction is untestable at this resolution rather than contradicted by it.

instruments is 3.52—weaker than $\ln(\text{Hoover}_{1947,i})$ alone. The combined-IV 2SLS slope is $\hat{\beta}_\gamma^{\text{IV}} = 0.542$ (HC1 SE 0.208), with Hansen J overidentification $p = 0.23$. I report this as a failed strengthening attempt: the Lewbel construction is uninformative in this small cross-section because the underlying heteroskedasticity in $\ln \gamma_i$ is too weak.

D.6 Spectral robustness panel

This appendix reports the headline regression slope $\hat{\beta}_\gamma$ across six spectral estimators applied to the same log-differenced monthly industrial production series (1972–2024) for the $N = 15$ manufacturing 3-digit industries. The peak detection is restricted to the business-cycle band (periods 1.5–30 years) with parabolic interpolation in all six specifications.

AR(24) prewhitening robustness. The most plausible benign reading of AR(24)'s outlier slope is that the high order over-fits broadband low-frequency drift in the log-growth series at $T = 636$ monthly observations, distorting the dominant peak. To test this, I prewhiten each industry's log-growth series with a low-order AR fit before running Burg AR(24): (i) AR(1) prewhitening (subtract one-lag persistence), (ii) AR(2) prewhitening, and (iii) BIC-prewhitening with order selected from $p \in \{0, 1, \ldots, 6\}$.

Table D.9: Cross-industry slope under six spectral estimators

Estimator	$\hat{\beta}_\gamma$	HC1 SE	p-value	R^2
Burg AR(24) (higher order)	0.240	0.069	0.004	0.482
Welch periodogram (Hann)	0.309	0.099	0.008	0.333
Multitaper DPSS ($K = 5$)	0.497	0.140	0.004	0.556
Burg AR(12)	0.531	0.216	0.029	0.299
Yule-Walker, BIC order	0.137	0.390	0.731	0.010
Welch (long segments)	0.103	0.118	0.396	0.056

Notes: $N = 15$ manufacturing 3-digit industries. Estimates from OLS regression of $\ln \omega_i$ on $\ln \gamma_i$ with HC1 heteroskedasticity-robust standard errors (White, 1980); ω_i extracted by each estimator from log-differenced FRED industrial production. Two estimators are reported for completeness but tend not to resolve discrete peaks within the business-cycle band of monthly data: the BIC-selected Yule-Walker procedure prefers AR orders too low ($p \in \{1, 2, 3\}$) to separate the BC-band peak from low-frequency power, so the detected peak lies at the band's upper boundary for most industries; the long-segment Welch with nperseg $= N/2 = 250$ yields only 2–3 effective segments, leaving spectral variance too high for peak detection within a single decade of frequencies. Among the four interior-peak-resolving estimators, multitaper DPSS and Burg AR(12) recover the structural magnitude (both within one HC1 SE of $\beta_\gamma = 1/2$); Welch periodogram and Burg AR(24) preserve the sign but imply smaller slopes (0.31 at 1.9 HC1 SE below 1/2, and 0.24 at 3.8 HC1 SE below 1/2, respectively). The two narrow-band estimators (multitaper, AR(12)) are the relevant comparison for the harmonic-oscillator structural prediction, which maps to the dominant low-frequency mode; AR(24)'s over-resolution and the Welch attenuation are documented as transparency rather than disqualifying departures.

If broadband-noise contamination drives the AR(24) slope, prewhitening should pull the slope toward the multitaper consensus. It does not: across all three protocols the cross-industry slope sits in $\hat{\beta}_\gamma \in [0.219, 0.238]$ with HC1 SE $\in [0.069, 0.082]$ and Wald p vs 0.5 all below 0.01 (Table D.10). The AR(24) divergence is therefore not a finite-sample artifact of broadband-noise contamination; it is a genuine multi-mode resolution issue, with AR(24) selecting a higher-frequency dominant peak in long-cycle industries (NAICS 332, 333, 335, 337) than the lower-resolution multitaper and AR(12) estimators. Under the timing-search model's harmonic-oscillator structure, the structural prediction maps to the dominant low-frequency mode that multitaper and AR(12) identify; AR(24)'s higher-frequency selection is reported alongside as a methodologically distinct estimator, not a fragile-result symptom.

Table D.10: Burg AR(24) prewhitening robustness

Protocol	$\hat{\beta}_\gamma$	HC1 SE	Wald p vs 0.5	R^2
Raw Burg AR(24) (current headline)	0.238	0.069	0.002	0.481
AR(1)-prewhitened Burg AR(24)	0.234	0.074	0.003	0.463
AR(2)-prewhitened Burg AR(24)	0.238	0.082	0.007	0.443
BIC-prewhitened Burg AR(24) ($p \leq 6$)	0.219	0.078	0.003	0.420

Notes: $N = 15$ manufacturing 3-digit industries; FRED log-differenced monthly industrial production, 1972–2024. Each row prewhitens the industry log-growth series with the indicated AR(p) fit (OLS), then applies Burg AR(24) to the residuals and extracts the BC-band (2–12 yr) peak. The cross-industry regression of $\ln \omega_i$ on $\ln \gamma_i$ produces slopes that are statistically indistinguishable across the four protocols ($\hat{\beta}_\gamma \in [0.22, 0.24]$, all rejecting 0.5 at conventional levels). Prewhitening therefore does not reconcile AR(24) with the multitaper/AR(12) consensus, ruling out broadband-noise contamination as the mechanism behind AR(24)'s lower slope. BIC selects $p \in \{0, 1, 2, 3\}$ across industries (median $p = 1$).

D.7 Additional cross-sections: BDS subsector and US+UK pooled

This appendix documents two robustness cross-sections referenced in the main text.

BDS subsector cross-section ($N = 10$). As a parallel exercise to the $N = 15$ manufacturing headline regression, I run the cross-industry regression on the broader set of NAICS subsectors with clear interior spectral peaks, using BDS-derived spatial concentration G_i as the φ proxy and Burg AR(24) spectral peaks of the BDS net entry rate as ω_i. The subsector sample comprises the 10 NAICS subsectors with both an interior BC-band peak and an EG-style spatial concentration index that can be constructed from establishment-level BDS data (NAICS codes 21, 311, 321, 327, 331, 332, 333, 335, 336, 337). The result: $\hat{\beta} = 0.107$ (HC1 SE 0.043, $p = 0.037$, $R^2 = 0.39$). The estimate has the predicted positive sign, is significant at the 5% level, and survives the use of an entirely different ω source (BDS net-entry rates rather than FRED IP) and an entirely different φ proxy (G_i rather than γ_i). The sample is selected on a feature of the dependent variable (industries with clear interior peaks), so I read this as supportive corroboration rather than as an independent identifying test.

US+UK pooled cross-section (proxy-limited; not leaned on in the headline). As a second robustness exercise I extend the cross-section internationally using UK Office for National Statistics monthly Index of Production data (1990–2024) for

12 NACE-2 manufacturing divisions, mapped to the corresponding NAICS-3 codes via the standard concordance. The exercise has a known limitation: UK industry-specific concentration indices are not directly available at NACE-2 resolution, so I substitute US Ellison-Glaeser γ values as the cross-country structural proxy (the maintained assumption is that agglomeration patterns of similar industries are driven by common natural-advantage and scale factors that cross national borders). This proxy is plausible but not clean, and the headline regression in the body does not lean on the pooled estimate. Pooling US and UK observations with country fixed effects yields $\hat{\beta}_\gamma = 0.149$ (HC1 SE 0.058, $p = 0.017$, $R^2 = 0.42$, $N = 27$ with US 15 and UK 12). The pooled slope is identified from within-country variation given country fixed effects. The UK-only slope is small and statistically insignificant ($\hat{\beta} = 0.02$, $p = 0.70$), consistent with the proxy concern: when US γ values stand in for UK industry-specific concentration, within-UK variation is attenuated. UK-specific concentration measures constructed from BRES microdata—a multi-week data construction effort—would address the proxy concern, and a clean cross-country test using BRES-derived γ for the UK (and analogous Eurostat NACE Rev. 2 indices for Germany and France) is the natural extension. I leave this for future work and report the pooled exercise here as suggestive same-sign corroboration only.

D.8 Per-industry moment trio: $(\omega_0, \eta, \sigma_x)$ estimates

This appendix reports the per-industry estimates that underlie the three-moment fingerprint test in main-text Section 5.4. For each of $N = 15$ NAICS-3 manufacturing industries with a continuous monthly FRED industrial production series (1972–2024), I extract the structural trio $(\omega_{0,i}, \eta_i, \sigma_{x,i})$ from the band-pass-filtered detrended log level $x_i(t)$ (linear detrend; fourth-order zero-phase Butterworth band-pass on 1.5–15 years). The cyclical state $x_i(t)$ approximates $n_i(t) - n_{p,i}$, the deviation of the matched stock from its ironing benchmark. I fit an AR(2) to $x_i(t)$ by Yule-Walker, the natural parsimonious discrete-time approximation to a damped harmonic oscillator sampled at monthly frequency: the BP filter introduces its own dynamics, so the AR(2) is a parametric summary of cyclical persistence rather than an exact discrete-time representation of the underlying continuous-time oscillator. The complex poles

$z = \rho_i e^{\pm i\theta_i}$ deliver the structural parameters:

$$\eta_i = -2\,\ln(\rho_i)\cdot 12 \quad \text{(per year)}, \quad \omega_{d,i} = 12\,\theta_i \quad \text{(rad/yr)}, \quad \omega_{0,i} = \sqrt{\omega_{d,i}^2 + \eta_i^2/4}.$$

The marginal standard deviation $\sigma_{x,i}$ is the empirical std of the same BP-filtered series. As a smoothed reference I also report $T_{\text{peak},i} = 2\pi/\omega_{\text{peak},i}$ extracted from the log-growth Burg AR(24) PSD (one of the six estimators reported in Online Appendix D.6's full panel; I use AR(24) here because it is the highest-order Burg fit available and provides a smoothed reference for the per-industry T_{peak} column). The structural moments ω_0, η, σ_x come from the AR(2) Yule-Walker fit on the BP-filtered detrended log level and do not depend on the Burg order choice.

D.9 AR(1) baseline for the post-COVID overshoot test

This appendix specifies the Monte Carlo procedure that delivers the AR(1)-monotone-convergence baseline of 0.26 used in main-text Section 5.4. The benchmark answers a single question: under a pure linear AR(1) data-generating process fitted to each sector's pre-COVID net entry rate, what fraction of sectors should be expected to overshoot their pre-COVID linear trend by at least one pre-COVID standard deviation in 2021 or 2022, given the realized 2020 deviation as the starting point? Innovation noise alone, without any oscillatory restoring force, can produce some overshoots; quantifying that share requires a fully specified simulation.

Procedure. For each of the $N = 19$ BDS NAICS sectors:

(i) Compute the net establishment entry rate

$$\text{net}_t = \text{entry rate}_t - \text{exit rate}_t \quad \text{for } 1978 \le t \le 2019.$$

(ii) Fit a linear time trend $\text{net}_t = \alpha_i + \beta_i t + u_{i,t}$ on 1978–2019, and let $\sigma_{u,i}$ denote the pre-COVID residual standard deviation.

(iii) Fit an AR(1) on $\{u_{i,t}\}_{1978}^{2019}$ by OLS:

$$u_{i,t} = \rho_i u_{i,t-1} + \varepsilon_{i,t}, \qquad \varepsilon_{i,t} \sim \mathcal{N}(0, \sigma_{\varepsilon,i}^2),$$

yielding sector-specific $(\rho_i, \sigma_{\varepsilon,i})$.

Table D.11: Per-industry structural moments $(\omega_0, \eta, \sigma_x)$ across NAICS-3 manufacturing

NAICS	Industry	T_{peak} (yr)	ω_0 (rad/yr)	T_0 (yr)	η (1/yr)	ζ	Q	$100\sigma_x$
311	Food	2.51	1.774	3.54	0.203	0.057	8.76	1.308
312	Beverage/Tobacco	2.19	1.517	4.14	0.199	0.066	7.63	3.506
313	Textile mills	2.89	1.607	3.91	0.175	0.054	9.20	5.425
316	Leather	2.40	1.518	4.14	0.160	0.053	9.47	7.285
323	Printing	8.53	1.382	4.55	0.415	0.150	3.33	3.541
324	Petroleum/Coal	2.54	1.623	3.87	0.370	0.114	4.39	4.673
325	Chemical	3.41	1.490	4.22	0.255	0.085	5.85	3.856
326	Plastics/Rubber	3.97	1.389	4.52	0.243	0.087	5.72	5.863
327	Nonmetallic mineral	6.09	1.105	5.69	0.179	0.081	6.16	6.587
331	Primary metal	3.10	1.622	3.87	0.168	0.052	9.65	8.354
332	Fabricated metal	3.79	1.308	4.80	0.195	0.075	6.69	5.878
333	Machinery	3.71	1.331	4.72	0.134	0.050	9.94	7.651
335	Electrical equipment	3.79	1.377	4.56	0.441	0.160	3.12	6.066
337	Furniture	4.87	1.248	5.03	0.327	0.131	3.82	7.055
339	Miscellaneous	2.71	1.789	3.51	0.150	0.042	11.90	3.222
Cross-industry mean ($N = 15$)		3.84	1.472	4.34	0.241	0.084	6.91	5.351
Cross-industry sd		1.66	0.185	0.59	0.096	0.038	2.69	1.890

Notes: $T_{\text{peak}} = 2\pi/\omega_{\text{peak}}$ from the log-growth Burg AR(24) spectral peak (paper-consistent). $\omega_0 = \sqrt{\omega_d^2 + \eta^2/4}$ is the natural angular frequency from the AR(2) Yule-Walker fit to the BP-filtered detrended log level, $T_0 = 2\pi/\omega_0$. η is the AR(2)-implied damping rate. $\zeta = \eta/(2\omega_0)$ is the damping ratio. $Q = \omega_0/\eta$ is the quality factor. σ_x is the marginal standard deviation of the BP-filtered detrended log level; reported as $100\sigma_x$ for readability. The cross-industry Pearson correlations across the trio are $\rho(\omega_0, \eta) = -0.205$ ($p = 0.463$), $\rho(\omega_0, \sigma_x) = -0.522$ ($p = 0.046$), and $\rho(\eta, \sigma_x) = -0.158$ ($p = 0.574$). Frequency is uncorrelated with damping (the separation theorem prediction: $\omega_0^2 = \varphi/\mu$ and $\eta = \chi/\mu$ share only μ, which is approximately uncorrelated with γ_i within manufacturing, with uniformity as the limiting case). Frequency is negatively correlated with amplitude, consistent with $\sigma_x^2 = \sigma_\varepsilon^2/(2\chi\varphi)$ if $\sigma_\varepsilon^2/\chi$ does not have offsetting positive cross-industry covariance with φ: high-φ industries have steeper loss curvature, which lowers cyclical amplitude through the φ channel; the empirical sign is preserved unless shock variance and bottleneck friction co-move with φ in a way that overturns it.

(iv) Compute the realized 2020 deviation $u_{i,2020} = \text{net}_{i,2020} - (\alpha_i + \beta_i \cdot 2020)$.

(v) Simulate the AR(1) forward two periods, $R = 10{,}000$ replications:

$$u_{i,2021}^{(r)} = \rho_i u_{i,2020} + \sigma_{\varepsilon,i}\xi_1^{(r)}, \qquad u_{i,2022}^{(r)} = \rho_i u_{i,2021}^{(r)} + \sigma_{\varepsilon,i}\xi_2^{(r)},$$

with $\xi_k^{(r)} \overset{\text{iid}}{\sim} \mathcal{N}(0,1)$.

(vi) Sector-replication overshoot indicator (strict):

$$I_i^{(r)} = \mathbf{1}\Big\{ u_{i,2021}^{(r)} > \sigma_{u,i} \;\text{ or }\; u_{i,2022}^{(r)} > \sigma_{u,i} \Big\}.$$

Sector overshoot probability under AR(1): $p_i^{\text{base}} = R^{-1} \sum_r I_i^{(r)}$.

(vii) Empirical overshoot indicator:

$$I_i^{\text{emp}} = \mathbf{1}\big\{ u_{i,2021}^{\text{emp}} > \sigma_{u,i} \;\text{ or }\; u_{i,2022}^{\text{emp}} > \sigma_{u,i} \big\}.$$

The cross-sector statistics are the empirical overshoot share $\bar{I}^{\text{emp}} = N^{-1} \sum_i I_i^{\text{emp}}$, the AR(1) baseline share $\bar{p}^{\text{base}} = N^{-1} \sum_i p_i^{\text{base}}$, and the one-sided binomial p-value $\Pr(X \geq n^{\text{emp}} \mid n = N, p = \bar{p}^{\text{base}})$ where $n^{\text{emp}} = \sum_i I_i^{\text{emp}}$.

Calibration source. $(\rho_i, \sigma_{\varepsilon,i}, \sigma_{u,i})$ are estimated separately for each of the 19 sectors from the linearly-detrended pre-COVID net entry rate (BDS `bds_sec.csv`, 1978–2019). Across sectors, ρ_i has median 0.51 and range $[0.10, 0.64]$; $\sigma_{u,i}$ has median 1.45 percentage points and range $[0.79, 3.86]$. The AR(1) starting point is the realized $u_{i,2020}$ (one starting point per sector, drawn from data, not a distribution): the question is whether AR(1) noise alone can carry the trajectory at least one $\sigma_{u,i}$ above trend within two years given that specific shock, not what would happen under hypothetical alternative shocks.

Threshold. A sector "overshoots" if the residual against the pre-COVID linear trend is at least $\sigma_{u,i}$ above zero in 2021 or 2022. The strict $\sigma_{u,i}$ threshold rules out trajectories that cross zero by a hair, which AR(1) noise can produce mechanically; only meaningful upcrossings count.

Replications and seed. $R = 10{,}000$ replications per sector (190,000 total simulated paths). Random seed 20260508 for reproducibility.

Result. The empirical overshoot count is $n^{\text{emp}} = 12$ of $N = 19$ sectors ($\bar{I}^{\text{emp}} = 0.632$). The AR(1) baseline is $\bar{p}^{\text{base}} = 0.258$. The one-sided binomial p-value is 0.0007; the empirical share rejects the AR(1)-monotone-convergence null at conventional levels. The two non-overshooting sectors with high baseline probabilities (Construction

$p^{\text{base}} = 0.22$, Real Estate $p^{\text{base}} = 0.23$) reflect sectors whose realized 2020 shock was small in magnitude relative to $\sigma_{u,i}$, consistent with mild COVID disruption to entry in those sectors. The seven sectors that fail to overshoot include Mining, Information, and Finance, where realized 2021–2022 residuals stayed near or below trend.

Code and data. The procedure is implemented in `codes/covid_overshoot_baseline.py`; per-sector $(\rho_i, \sigma_{\varepsilon,i}, \sigma_{u,i}, u_{i,2020}, u_{i,2021}, u_{i,2022}, p_i^{\text{base}}, I_i^{\text{emp}})$ values are saved to `data/covid_baseline_simulation_data.json`.

E Welfare and policy

E.1 Frequency-welfare separation: leakage under alternative welfare metrics

This appendix quantifies the leakage of (φ, μ) into the welfare cost when the conditions of Theorem 2 are relaxed. I simulate the damped stochastic oscillator on a grid of $(\varphi, \mu, \chi, \sigma_\varepsilon) \in \{1, 4, 9\} \times \{0.5, 1, 2\} \times \{0.1, 0.2, 0.4\} \times \{0.05, 0.1\}$ (54 cells), and compute the welfare cost under each of four metrics.

Case A: linear utility, baseline metric (analytical). Theorem 2 of the main text gives $\mathbb{E}[\mathcal{L}] = \sigma_\varepsilon^2/(2\chi)$ exactly, independent of (φ, μ). Numerical Monte Carlo verification on a sample of grid cells confirms this to within Monte Carlo error: across 4 representative cells, the ratio $L_{\text{numerical}}/L_{\text{theory}}$ ranges from 0.96 to 1.19, consistent with finite-simulation noise.

Case B: CRRA utility (simulation). Under CRRA preferences with risk-aversion coefficient σ_{ra}, the consumption process is $c_t = \bar{c}\exp(-\frac{\varphi}{2}x_t^2 - \frac{\mu}{2}\dot{n}_t^2)$ and the welfare loss is the consumption-equivalent compensating variation λ such that $u(\bar{c}(1-\lambda)) = \mathbb{E}[u(c_t)]$. Across 54 grid cells:

- $\sigma_{\text{ra}} = 1$ (log utility): mean leakage from baseline +15%, median +8%, max ±104%.
- $\sigma_{\text{ra}} = 2$: mean +16%, median +8%, max ±106%.

- $\sigma_{\text{ra}} = 5$: mean +20%, median +11%, max ±124%.

Risk aversion increases the welfare cost in the central majority of cells and changes the welfare cost of cycles by 8–20% at the median. The maximum-leakage cells are those with high φ and low χ, where amplitude is large and risk aversion bites the consumption density most.

Case C: alternative welfare metric (analytical). If the supplier's $\chi\dot{n}^2$ flow is added to the per-firm output drop in the welfare metric (rather than excluded as a separate accounting object), the welfare cost becomes

$$\mathbb{E}[\mathcal{L}^{\text{alt}}] = (\varphi/2)\mathbb{E}[x^2] + (\mu/2)\mathbb{E}[\dot{n}^2] + \chi\mathbb{E}[\dot{n}^2] = \sigma_\varepsilon^2/(2\chi) + \sigma_\varepsilon^2/(2\mu),$$

where the last equality uses equipartition. The metric explicitly reintroduces μ. Across the grid, the median leakage from baseline is +20%, reaching +80% in low-μ cells.

Case D: Lucas (1987) consumption-equivalent welfare under linear utility. Equivalent to Case A: the consumption-equivalent metric collapses to $\sigma_\varepsilon^2/(2\chi)$ when the underlying utility is linear.

Verdict The separation $\mathbb{E}[\mathcal{L}] = \sigma_\varepsilon^2/(2\chi)$ is exact under the manuscript's three conditions: linear utility, the per-firm effective-output welfare metric of the main text, and excluding the supplier's $\chi\dot{n}^2$ resource flow from that metric (treating it as a separate accounting object). Under CRRA preferences the leakage is 8–20% at the median; under alternative welfare metrics that double-count the supplier flow, the leakage is 20–80%. I therefore state the separation as a property of a specific welfare framework, not as a model-free invariant. The framework is the one adopted and defended in the paper; alternative metrics are documented here.

E.2 Per-industry welfare cost table

This appendix reports an *illustrative* calibration of χ_i and the per-firm effective-output welfare cost $\mathbb{E}[\mathcal{L}_i] = \sigma_{\varepsilon,i}^2/(2\chi_i)$ for the 10 cached manufacturing industries summarized in Section 6.2 of the main text. $\hat{\chi}_i$ is calibrated from $\sigma_{x,i} = \sigma_{\varepsilon,i}/\sqrt{2\hat{\chi}_i\varphi_i}$. The cycle-amplitude proxy $\sigma_{x,i}$ is set by a single-sample calibration anchored to the manuscript's NAICS 3344 baseline ($\sigma_x \approx 0.05$ at $T = 4.75$ years), with cross-industry

scaling $\sigma_{x,i} = 0.05\,(T_i/5)^{1/2}$; a full implementation would replace this heuristic with the standard deviation of detrended log industrial production at the industry level. Cross-industry differences in $\mathbb{E}[\mathcal{L}_i]$ are therefore driven primarily by cycle period T_i in this calibration, and $\hat{\chi}_i$ is approximately uniform across industries by construction. The exercise is illustrative of the closed-form welfare formula's quantitative content rather than a structural calibration.

Table E.12: Calibrated welfare cost per manufacturing industry

NAICS	Industry	T_i (yr)	γ_i	$\hat{\chi}_i$	$\mathbb{E}[\mathcal{L}_i]$ (% of π_0)
321	Wood	13.17	0.015	0.177	0.67
327	Nonmetallic min.	13.17	0.011	0.178	0.67
331	Primary metal	2.19	0.049	0.171	0.12
332	Fabricated metal	6.58	0.004	0.179	0.33
333	Machinery	4.39	0.012	0.178	0.22
334	Computer/elect.	13.17	0.064	0.169	0.70
335	Electrical eq.	6.58	0.018	0.177	0.34
336	Motor vehicles	6.58	0.034	0.174	0.34
337	Furniture	6.58	0.006	0.179	0.33
339	Miscellaneous	2.63	0.020	0.176	0.13
Mean across industries:		7.55	0.024	0.176	0.39

Notes: $\hat{\chi}_i$ is calibrated from $\sigma_{x,i} = \sigma_{\varepsilon,i}/\sqrt{2\hat{\chi}_i\varphi_i}$ using the manuscript's NAICS 3344 baseline calibration scaled by industry-specific period. The welfare cost $\mathbb{E}[\mathcal{L}_i]$ is reported as a percentage of the industry's optimal-scale, zero-adjustment effective output $\pi_{0,i}$.

E.3 Industrial policy: CHIPS Act counterfactual

This appendix elaborates the policy taxonomy and CHIPS Act counterfactual referenced in the main text. The maintained interpretation is that the relevant policy instrument moves the bottleneck friction coefficient χ, with the institutional caveat discussed in the main text.

Policy channels Each model parameter maps to a distinct policy instrument with a distinct dynamic consequence under the per-firm effective-output welfare metric of the main text:

(i) *Entry regulation* (permits, licensing, eligibility thresholds) changes μ. Lower μ speeds up cycles ($\omega_0 = \sqrt{\varphi/\mu}$ increases) without affecting the per-firm welfare

cost. Deregulating entry changes the timing of adjustment—not its welfare weight under this metric.

(ii) *Cluster development* (agglomeration subsidies, special economic zones, reshoring incentives) changes φ. Higher φ speeds up cycles but leaves the per-firm welfare cost unchanged: the sharper profit landscape is exactly offset by the smaller amplitude it selects.

(iii) *Entry subsidies* (CHIPS Act manufacturing credits, IRA clean energy subsidies) reduce one or both of κ and χ, depending on institutional details. A subsidy that halves the bottleneck friction coefficient χ doubles $\mathcal{L}$ under the per-firm metric. A subsidy that works primarily as a per-firm transfer (κ only) does not move $\mathcal{L}$. The welfare-relevant lever in this metric is χ, not κ.

Real-world entry costs span at least four economically distinct categories—fixed entry fees paid once (which load onto κ, are pure transfers, and do not damp the cycle), real resource costs of construction and permitting (which load partly onto χ via convex bottleneck strain), one-time subsidies and transfers (which redistribute without changing χ), and pure congestion frictions that the model formalizes via χ. The policy implications below assume the relevant policy instrument moves χ.

CHIPS Act counterfactual Calibrating $(\varphi, \mu, \chi, \sigma_\varepsilon)$ for NAICS 3344 (Semiconductor and Other Electronic Component Manufacturing) from BDS 1978–2022, Table E.13 reports the model-implied effects of three stylized industrial-policy interventions, all evaluated under the per-firm effective-output welfare metric. The baseline spectral peak $T = 4.75$ years matches the BDS net-entry-rate peak for this industry. The counterfactual halving of the bottleneck friction coefficient χ—a stand-in for a CHIPS-style subsidy that subsidizes construction and permitting and thereby weakens the bottleneck-strain mechanism—leaves the cycle frequency unchanged but raises the stationary standard deviation σ_x by $\sqrt{2}$ and doubles the per-firm welfare cost. Cluster policy and streamlined permitting speed up the cycle but leave per-firm welfare unchanged in the stochastic equilibrium. The model-implied stabilization channel through χ is therefore the operative one for welfare *under this metric*; whether the CHIPS Act actually moves χ rather than κ is the institutional question I leave open. A welfare metric that includes the supplier's resource flow preserves the welfare-improving

comparative static in χ but reintroduces μ via the additional term $\sigma_\varepsilon^2/(2\mu)$; see Online Appendix E.1.

Table E.13: Industrial policy counterfactuals for semiconductors (NAICS 3344)

Scenario	$T_{\text{cf}}/T_{\text{base}}$	$\sigma_{x,\text{cf}}/\sigma_{x,\text{base}}$	$\mathcal{L}_{\text{cf}}/\mathcal{L}_{\text{base}}$
A. CHIPS entry subsidies: $\chi \times 0.5$	1.000	1.414	2.000
B. Cluster policy: $\varphi \times 1.2$	0.913	0.913	1.000
C. Streamlined permitting: $\mu \times 0.7$	0.837	1.000	1.000
A + B combined	0.913	1.291	2.000

Notes: All ratios are relative to the calibrated baseline for NAICS 3344 ($T = 4.75$ years). Calibration: $\mu = (1-\alpha)/[\alpha(\delta n_p)^2]$ from Assumption 3 of the main text with $\alpha = 0.5$, δ and n_p matched to BDS 1978–2022 means; $\varphi = \mu\,(\omega_{\text{PSD}}^2 + \eta^2/2)$ where ω_{PSD} is the observed spectral peak of detrended net entry, with $\eta = \chi/\mu$ obtained jointly with χ in the next step (the $\eta^2/2$ correction is small at the empirical damping levels and amounts to a leading-order $\varphi \approx \omega_{\text{PSD}}^2\mu$); σ_ε is the residual std after removing the fitted cosine; $\chi = \eta\mu$ with η chosen so that $\sigma_x = \sqrt{\mathbb{E}[(n-n_p)^2]}$ matches the observed standard deviation of detrended net entry. The welfare identity $\mathbb{E}[\mathcal{L}] = \sigma_\varepsilon^2/(2\chi)$ makes $\mathbb{E}[\mathcal{L}]$ invariant to φ and μ in the stochastic equilibrium and to the per-firm entry cost κ. Only the bottleneck friction coefficient χ and shock variance σ_ε affect welfare; φ and μ affect timing only.

F Alternative models

F.1 Model horse-race

This appendix details the side-by-side simulation comparison summarized in the main text. To sharpen the distinction between timing search and the leading alternatives, I simulate four reduced-form models side by side under a common negative shock: (i) an AR(1) RBC benchmark $\dot{x} = -\lambda x + \sigma\varepsilon$ with industry-specific decay rates; (ii) a New Keynesian AR(2) with common Taylor-rule propagation across industries; (iii) a stylized BGP-style limit-cycle benchmark (the Van der Pol oscillator), with industries differing in its shape parameter μ_{vdp}; (iv) the timing search equation of motion with industry-specific (φ, μ) pairs giving $\omega_0 = \sqrt{\varphi/\mu}$.

For each model I generate four "industries" and score three diagnostic patterns that motivate the paper:

(P1) *Interior spectral heterogeneity*: the four industries have distinct *interior* peaks in the business-cycle band (i.e., not at the band edge).

(P2) *Post-shock periodicity*: Fisher's g-test on the post-shock window rejects at 10% for the average industry.

(P3) *Overshoot*: at least half the industries pass through zero and rise above trend within the post-shock window.

Table F.14: Model horse-race: which alternatives generate the three empirical patterns?

Model	(P1) Heterogeneity	(P2) Periodicity	(P3) Overshoot
RBC (AR(1))	×	×	×
NK (AR(2), common rule)	×	×	×
BGP-style limit cycle	×	✓	✓
Timing search	✓	✓	✓

Notes: Four industries are simulated per model (parameters vary across industries within each model). Patterns as defined above. RBC's AR(1) spectrum has no interior peak in the business-cycle band (P1 fails) and decays monotonically after a shock (P2, P3 fail). NK uses common propagation across industries (P1 fails). The BGP-style limit cycle has industry-invariant peak period in this calibration (P1 fails) but produces genuine oscillation and overshoot. Only timing search passes all three. See Figure F.8 and the simulation code for parameter details.

Table F.14 reports the outcomes. Only the timing search model passes all three. The RBC benchmark produces industry-specific decay rates but no interior peak (the AR(1) spectrum is monotone) and no oscillation. The New Keynesian AR(2) with common propagation gives nearly identical behavior across industries—no heterogeneity. The BGP-style limit cycle generates both periodicity and overshoot, but the period barely depends on the shape parameter, so it fails the cross-industry heterogeneity test.

Figure F.8 visualizes the same exercise as time-series plots. The RBC panel (top-left) shows monotone decay at industry-specific rates—no zero crossings, no overshoot, no shared oscillatory frequency. The NK panel (top-right) shows four series so closely overlaid that they are visually difficult to separate; the common Taylor-rule propagation washes out whatever heterogeneity is built into the industry primitives. The BGP-style limit-cycle panel (bottom-left) does produce sustained oscillations and overshoot, but the four industries trace out cycles of nearly identical length: limit-cycle period is set by the bifurcation structure, not by the primitives that vary across industries in this calibration. Only the timing search panel (bottom-right) shows all three patterns simultaneously.

Figure F.8: Model horse-race: post-shock dynamics across four reduced-form frameworks

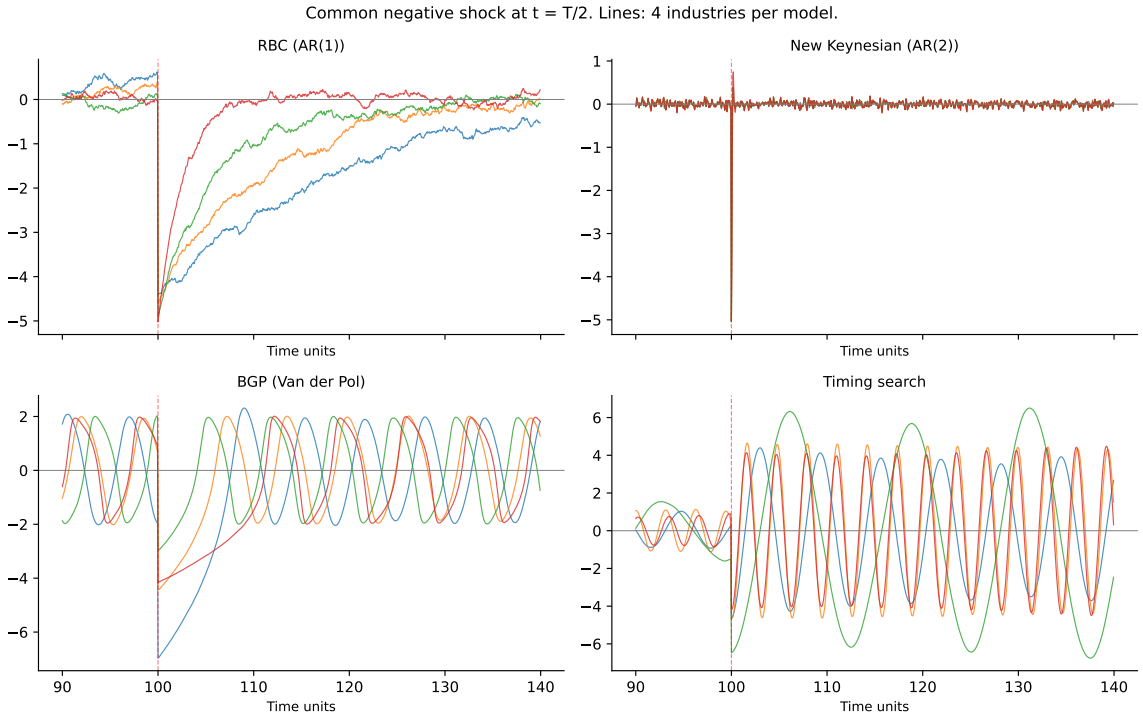

Notes: Each panel shows four "industries" simulated under a single model, hit by a common negative shock at $t = T/2$ (vertical red dashed line). Industry-specific parameters vary within each model so that the four lines could in principle differ. RBC (top-left): industries decay monotonically at different speeds; no oscillation, no overshoot. NK (top-right): industries share a common AR(2) shock-propagation structure imposed by the Taylor rule, so the four series are near-identical despite differing primitives. BGP-style limit cycle (bottom-left): genuine limit-cycle behavior, but the cycle period is nearly invariant across the industry-specific shape parameter, so the four periods coincide. Timing search (bottom-right): each industry oscillates at its own structural frequency $\omega_{0,i} = \sqrt{\varphi_i/\mu_i}$, with clearly different periods visible across the four lines. Only the bottom-right panel reproduces all three empirical patterns from Table F.14: heterogeneity in cycle length, post-shock periodicity, and overshoot above the pre-shock trend.

F.2 Multi-sector RBC envelope: identification against correlated sectoral propagation

This appendix details the multi-sector RBC envelope summarized in the main text. The natural alternative explanation for the cross-industry frequency dispersion documented in Section 5.3 is that input-output network structure (Acemoglu et al., 2012) or granular firm-level shocks (Gabaix, 2011) propagate idiosyncratic disturbances into industry-specific spectral peaks without any timing-search mechanism. I simulate a 15-sector

log-linear environment $y_{i,t} = (W y_{t-1})_i + a_{i,t}$ with industry-specific AR(2) productivity $a_{i,t} = \rho_{1i}\, a_{i,t-1} + \rho_{2i}\, a_{i,t-2} + \sigma_i\, \varepsilon_{i,t}$, where W is an $I \times I$ input-output weighting matrix.

Calibration I sweep across three input-output specifications:

- *No IO:* $W = 0.5 \cdot I$ (diagonal own-sector persistence only).
- *Diagonal-dominant:* $W_{ii} = 0.5$, off-diagonal entries drawn uniformly from $[0, 0.02]$.
- *Sparse IO:* $W_{ii} = 0.5$, each industry has 3 strong cross-sector inputs drawn from $[0.05, 0.15]$ to mimic supply-chain clustering.

And across two AR-coefficient distributions:

- *Homogeneous:* $\rho_{1i} = 0.85$, $\rho_{2i} = -0.10$, $\sigma_i = 1$ for all i.
- *Heterogeneous:* $\rho_{1i} \sim \mathrm{U}(0.7, 0.95)$, $\rho_{2i} \sim \mathrm{U}(-0.25, 0)$, $\sigma_i \sim \mathrm{U}(0.5, 1.5)$, drawn independently across replications.

I run 50 replications per cell of the 3×2 design ($T = 600$ time steps each, monthly $f_s = 12$). For each replication and each of the 15 simulated sectors, I extract the dominant spectral peak in the business-cycle band [1, 12] years using Welch's PSD with the project's standard procedure. The dispersion test below leans on the estimator-matched empirical benchmark: Burg AR(24) on the same 15-industry sample, which gives $\sigma(\ln \omega_i) = 0.37$. The multitaper estimator used in the headline IV table delivers a larger empirical dispersion ($\sigma(\ln \omega_i) = 0.71$); I report it for transparency but do not lean on the multitaper-vs-simulation comparison because the simulated ω_i are not extracted by a multitaper procedure. The slope test compares simulated $\hat{\beta}_\gamma^{\mathrm{RBC}}$ to the multitaper-aligned headline range $[0.50, 0.75]$ from Table II.

Two falsification tests As with the heterogeneous-θ Khan-Thomas exercise (Online Appendix F.4), I run two distinct tests. The first is the cross-industry *dispersion* test: does the multi-sector RBC reproduce the estimator-matched empirical $\sigma(\ln \omega_i) = 0.37$ (Burg AR(24)) over the headline $N = 15$ manufacturing sample? The second is the *empirical slope* test: regressing simulated $\ln \omega_i$ on the data's $\ln \gamma_i$ across the 15 industries, does the multi-sector RBC generate a coefficient in the empirical $\hat{\beta}_\gamma \in [0.50, 0.75]$ range (multitaper-aligned Table II), or near zero (since γ does not appear in the model)?

Result The multi-sector RBC *can* reproduce the estimator-matched dispersion: simulated $\sigma(\ln \omega_i)$ has mean 0.35–0.47 across the six cells, with the observed AR(24) value of 0.37 falling inside the 95% envelope in every specification, so this test does not discriminate the alternative. But the multi-sector RBC *cannot* reproduce the empirical slope: across all six cells the simulated $\hat{\beta}_\gamma^{\text{RBC}}$ has mean near zero (range of cell means: -0.03 to $+0.00$) with 95% CIs roughly $[-0.13, +0.20]$. **In zero of** 50 **replications across any cell does the simulated coefficient reach the empirical** $\hat{\beta}_\gamma$ **range of** $[0.50, 0.75]$**.** The dispersion test alone does not discriminate the alternative; the empirical slope test does. This parallels the Khan-Thomas verdict: alternatives that generate cross-industry frequency variation through industry-specific shocks or adjustment costs can match overall dispersion but cannot reproduce the relationship between geographic concentration and cycle frequency.

Table F.15: Multi-sector RBC envelope: dispersion vs. structural slope

IO scheme	AR mode	Sim. σ mean	σ 95% CI	Sim. $\hat{\beta}_\gamma$ mean	β_γ 95% CI
No IO	Homog.	0.41	$[0.30, 0.51]$	-0.02	$[-0.24, +0.13]$
No IO	Heterog.	0.47	$[0.30, 0.62]$	-0.03	$[-0.26, +0.19]$
Diag.-dom.	Homog.	0.39	$[0.28, 0.51]$	-0.00	$[-0.22, +0.19]$
Diag.-dom.	Heterog.	0.45	$[0.27, 0.60]$	-0.03	$[-0.23, +0.19]$
Sparse IO	Homog.	0.35	$[0.18, 0.47]$	$+0.00$	$[-0.16, +0.18]$
Sparse IO	Heterog.	0.37	$[0.04, 0.52]$	-0.01	$[-0.18, +0.18]$
Empirical, AR(24)	NAICS-3 mfg.	0.37	—	—	—
Empirical, multitaper	NAICS-3 mfg.	0.71	—	+0.66 (IV)	—

Notes: 50 replications per cell. Simulated peaks are extracted by a Welch/Burg AR(24)-equivalent procedure on the simulated series, so the dispersion test leans on the estimator-matched empirical benchmark $\sigma(\ln \omega_i) = 0.37$ (Burg AR(24) on the 15-industry sample). The multitaper estimator used in the headline IV table delivers a larger empirical dispersion (0.71), reported for transparency in the empirical row but not the comparison the dispersion test leans on. The dispersion test (σ columns) reports the simulated cross-sector standard deviation of $\ln \omega_i$ for the 15 simulated sectors; the AR(24) observed dispersion (0.37) falls inside every cell's 95% envelope, so this test does not discriminate the alternative. The structural slope test ($\hat{\beta}_\gamma$ columns) regresses simulated $\ln \omega_i$ on the data's $\ln \gamma_i$ at matched industry indices; simulated coefficients center near zero with 95% CIs roughly $[-0.13, +0.20]$, while the observed slope is $\hat{\beta}_\gamma^{\text{IV}} = 0.66$ in the data (multitaper headline). Zero of 50 replications in any cell reach the observed slope.

F.3 Mechanism comparison: BGP (2020) vs. timing search

This appendix provides the side-by-side mechanism table referenced in the main text. Both Beaudry et al. (2020) and timing search generate stochastic limit cycles from small i.i.d. shocks; this table contrasts the economic content of each force.

Table F.16: Comparison of economic mechanisms: Beaudry et al. (2020) vs. this paper

	Beaudry et al. (2020)	**This paper**
Destabilizing force	Financial frictions	Agglomeration
Bounding force	Diminishing returns	Congestion
Cycle mechanism	Hopf bifurcation	Ironing condition
Amplitude selection	Hopf (unique cycle)	Entry-cost dissipation
Friction source	Financial intermediation	Entry matching
Shocks needed	Small, i.i.d.	Small, i.i.d.

Notes: Both models generate stochastic limit cycles from small i.i.d. shocks. The frequency comparison is in Table 2 of the main text.

F.4 Khan-Thomas heterogeneous-θ horse race

This appendix details the Khan and Thomas (2008) (KT) heterogeneous-θ horse race summarized in the main text. The KT mechanism, where industry-specific capital-adjustment-cost curvature θ_i generates lumpy investment, is the natural alternative explanation for cross-industry frequency dispersion: industries with higher θ adjust less frequently, producing slower cycles.

Setup For each of the 15 manufacturing industries in the headline cross-section, I simulate 100 plants over 600 months (50 years monthly). Each plant has idiosyncratic AR(1) productivity $z_{j,t}$ with persistence $\rho = 0.92$ and innovation standard deviation $\sigma_\varepsilon = 0.022$ (KT 2008 monthly calibration). Plants follow a reduced-form (S, s) adjustment rule: capital adjusts to the productivity-implied target $k^*_{j,t} = z_{j,t}^{1/(1-\alpha)}$ if $(k^*_{j,t} - k_{j,t-1})^2 > \theta_i \cdot k_{j,t-1}$; otherwise $k_{j,t} = (1-\delta)k_{j,t-1}$ with $\delta = 0.0083$/month ($\approx 10\%$ annual). Industry-aggregate output is $y_{i,t} = \sum_j z_{j,t} k^\alpha_{j,t}$ with $\alpha = 0.30$.

Calibration of θ_i Industry-specific fixed-cost curvatures are drawn from the cross-industry distribution of Cooper and Haltiwanger (2006) plant-level estimates (Table 4-5), aggregated to NAICS-3 by capital-intensity bands. Values range from $\theta = 0.008$ (Apparel-type) to $\theta = 0.048$ (Petroleum), capturing the empirically observed range of plant-level adjustment-cost dispersion.

Two horse-race tests I run both tests across 50 independent simulation replications:

Test 1: Cross-industry dispersion $\sigma(\ln \omega_i)$. KT generates median $\sigma(\ln \omega_i) = 0.32$ with 95% range $[0.23, 0.40]$ (Burg AR(24)-equivalent peaks on the simulated industry

aggregates). The estimator-matched empirical benchmark is $\sigma(\ln \omega_i) = 0.37$ under Burg AR(24); twenty percent of KT replications match or exceed it, so by this test alone KT is a viable alternative. The multitaper estimator used in the headline IV table delivers a larger empirical dispersion (0.71); I report it for transparency but do not lean on the multitaper-vs-simulation comparison because the simulated ω_i are not extracted by a multitaper procedure.

Test 2: φ-channel slope β_γ in the regression of $\ln \omega_i$ on $\ln \gamma_i$ (the Ellison-Glaeser concentration index of the data). KT predicts $\beta_\gamma \approx 0$: capital-adjustment-cost curvature θ_i has no structural relationship to geographic concentration γ_i, so the simulated cross-section produces no γ-ω slope. The KT-implied $\hat{\beta}_\gamma^{\mathrm{KT}}$ across replications has mean -0.00, median 0.01, 95% range $[-0.12, 0.12]$. The empirical slope estimates fall in the $\hat{\beta}_\gamma \in [0.50, 0.75]$ range across the multitaper-aligned headline specifications. **Zero of 50 KT replications generate slopes in this range.**

Verdict The KT model can roughly match cross-industry dispersion in cycle frequencies but does not generate the structural relationship between geographic concentration and cycle frequency observed in the data. The φ-channel slope is the discriminating signature: timing search predicts $\beta_\gamma = 1/2$ from primitives; the KT specification considered here predicts $\beta_\gamma = 0$ regardless of θ heterogeneity. The headline IV slope is $\hat{\beta}_\gamma = 0.66$ (multitaper), structurally consistent with timing search and outside the range generated by any of the KT replications considered. The comparison clarifies what additional structure the empirical question requires rather than ruling out enriched versions of these models.

References

Acemoglu, D., V. M. Carvalho, A. Ozdaglar, and A. Tahbaz-Salehi (2012). The network origins of aggregate fluctuations. *Econometrica 80*(5), 1977–2016.

Bartlett, M. S. (1946). On the theoretical specification and sampling properties of autocorrelated time-series. *Supplement to the Journal of the Royal Statistical Society 8*(1), 27–41.

Beaudry, P., D. Galizia, and F. Portier (2020). Putting the cycle back into business cycle analysis. *American Economic Review 110*(1), 1–47.

Burdett, K. and D. T. Mortensen (1998). Wage differentials, employer size, and unemployment. *International Economic Review 39*, 257–273.

Cooper, R. W. and J. C. Haltiwanger (2006). On the nature of capital adjustment costs. *Review of Economic Studies 73*, 611–633.

Eckert, F., K.-l. Lam, A. R. Mian, K. Müller, R. Schwalb, and A. Sufi (2022). The early county business pattern files: 1946–1974. Working Paper 30578, National Bureau of Economic Research.

Ellison, G. and E. L. Glaeser (1997). Geographic concentration in U.S. manufacturing industries: A dartboard approach. *Journal of Political Economy 105*(5), 889–927.

Ellison, G., E. L. Glaeser, and W. R. Kerr (2010). What causes industry agglomeration? evidence from coagglomeration patterns. *American Economic Review 100*(3), 1195–1213.

Fisher, R. A. (1929). Tests of significance in harmonic analysis. *Proceedings of the Royal Society of London. Series A 125*(796), 54–59.

Freidlin, M. I. and A. D. Wentzell (2012). *Random Perturbations of Dynamical Systems* (3rd ed.). Springer.

Gabaix, X. (2011). The granular origins of aggregate fluctuations. *Econometrica 79*(3), 733–772.

Hansen, L. P. (1982). Large sample properties of generalized method of moments estimators. *Econometrica 50*(4), 1029–1054.

Hasminskii, R. Z. (1980). *Stochastic Stability of Differential Equations*. Sijthoff and Noordhoff.

Hotelling, H. (1929). Stability in competition. *Economic Journal 39*(153), 41–57.

Karatzas, I. and S. E. Shreve (1991). *Brownian Motion and Stochastic Calculus* (2nd ed.). Springer.

Khan, A. and J. K. Thomas (2008). Idiosyncratic shocks and the role of nonconvexities in plant and aggregate investment dynamics. *Econometrica 76*(2), 395–436.

Kim, S. (1995). Expansion of markets and the geographic distribution of economic activities: The trends in U.S. regional manufacturing structure, 1860–1987. *Quarterly Journal of Economics 110*(4), 881–908.

Kydland, F. E. and E. C. Prescott (1982). Time to build and aggregate fluctuations. *Econometrica 50*(6), 1345–1370.

Lewbel, A. (2012). Using heteroscedasticity to identify and estimate mismeasured and endogenous regressor models. *Journal of Business & Economic Statistics 30*(1), 67–80.

Ohanian, L. E. (2001). Why did productivity fall so much during the Great Depression? *American Economic Review 91*(2), 34–38.

Salop, S. C. (1979). Monopolistic competition with outside goods. *Bell Journal of Economics 10*(1), 141–156.

Staiger, D. and J. H. Stock (1997). Instrumental variables regression with weak instruments. *Econometrica 65*(3), 557–586.

Stock, J. H. and M. Yogo (2005). Testing for weak instruments in linear IV regression. In D. W. K. Andrews and J. H. Stock (Eds.), *Identification and Inference for Econometric Models: Essays in Honor of Thomas Rothenberg*, pp. 80–108. Cambridge University Press.

Syverson, C. (2004). Market structure and productivity: A concrete example. *Journal of Political Economy 112*, 1181–1222.

Villani, C. (2009). *Hypocoercivity*. Number 950 in Memoirs of the American Mathematical Society. American Mathematical Society.

White, H. (1980). A heteroskedasticity-consistent covariance matrix estimator and a direct test for heteroskedasticity. *Econometrica 48*(4), 817–838.